AD-A123 253 NUMERICAL CALCULATION OF THE PROPAGATION OF SPATIAL COHERENCE FROM PARTIALLY COHERENT SOURCES(U) HARRY DIAMOND LABS ADELPHI MD T H HOPP ET AL. OCT 82 1/1

UNCLASSIFIED HDL-TR-1979 F/G 12/1 NL

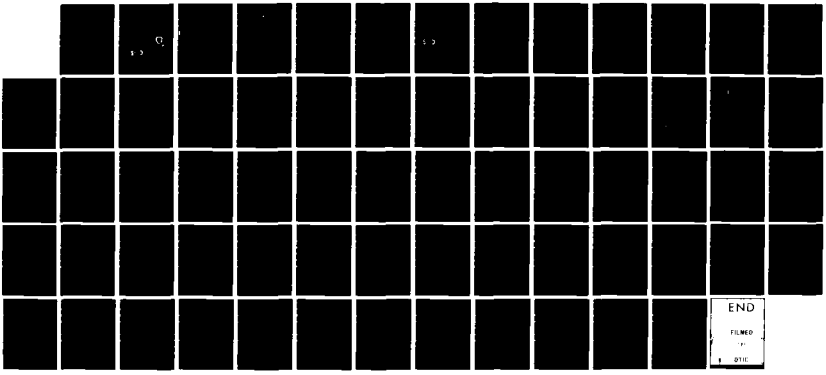

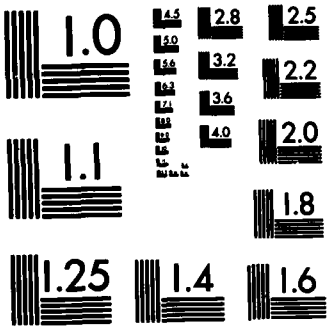

MICROCOPY RESOLUTION TEST CHART
NATIONAL BUREAU OF STANDARDS-1963-A

(12)

HDL-TR-1979
October 1982

AD A 123253

Numerical Calculation of the Propagation of Spatial Coherence from Partially Coherent Sources

Theodore H. Hopp
Dennis McGuire

DTIC
ELECTE
JAN 11 1983
S D
B

U.S. Army Electronics Research
and Development Command
Harry Diamond Laboratories
Adelphi, MD 20783

Approved for public release; distribution unlimited.

FILE COPY

83 01 11 008

The findings in this report are not to be construed as an official Department of the Army position unless so designated by other authorized documents.

Citation of manufacturers' or trade names does not constitute an official indorsement or approval of the use thereof.

Destroy this report when it is no longer needed. Do not return it to the originator.

UNCLASSIFIED

SECURITY CLASSIFICATION OF THIS PAGE (When Data Entered)

REPORT DOCUMENTATION PAGE		READ INSTRUCTIONS BEFORE COMPLETING FORM
1. REPORT NUMBER HDL-TR-1979	2. GOVT ACCESSION NO. AD-A123253	3. RECIPIENT'S CATALOG NUMBER
4. TITLE (and Subtitle) Numerical Calculation of the Propagation of Spatial Coherence from Partially Coherent Sources		5. TYPE OF REPORT & PERIOD COVERED Technical Report
		6. PERFORMING ORG. REPORT NUMBER
7. AUTHOR(s) Theodore H. Hopp Dennis McGuire		8. CONTRACT OR GRANT NUMBER(s) PRON: A18R010003A1A9
9. PERFORMING ORGANIZATION NAME AND ADDRESS Harry Diamond Laboratories 2800 Powder Mill Road Adelphi, MD 20783		10. PROGRAM ELEMENT, PROJECT, TASK AREA & WORK UNIT NUMBERS Program Ele: 61102
11. CONTROLLING OFFICE NAME AND ADDRESS U.S. Army Materiel Development and Readiness Command Alexandria, VA 22333		12. REPORT DATE October 1982
		13. NUMBER OF PAGES 66
14. MONITORING AGENCY NAME & ADDRESS(if different from Controlling Office)		15. SECURITY CLASS. (of this report) UNCLASSIFIED
		15a. DECLASSIFICATION/DOWNGRADING SCHEDULE

16. DISTRIBUTION STATEMENT (of this Report)

Approved for public release; distribution unlimited.

17. DISTRIBUTION STATEMENT (of the abstract entered in Block 20, if different from Report)

18. SUPPLEMENTARY NOTES

HDL Project: A44913
DRCMS Code: 611102H440011
DA Project: 1L161102AH44

19. KEY WORDS (Continue on reverse side if necessary and identify by block number)

Near-field diffraction	Rough surface reflections
Mutual intensity	Mutual coherence
Numerical integration	Oscillatory integrands
Physical optics	Fresnel diffraction
Optical heterodyne	Heterodyne detection

20. ABSTRACT (Continue on reverse side if necessary and identify by block number)

This report considers the numerical calculation of the mutual intensity function of highly coherent laser radiation after reflection from a surface having roughness on the scale of the laser wavelength and at arbitrary distances from the reflector. The mutual intensity function characterizes the second-order spatial coherence properties of the nearly monochromatic reflected field and is of interest for evaluating the potential of coherent detection schemes for optical fuzing systems.

DD FORM 1 JAN 73 1473 EDITION OF 1 NOV 65 IS OBSOLETE

UNCLASSIFIED

SECURITY CLASSIFICATION OF THIS PAGE (When Data Entered)

20. ABSTRACT (cont'd)

The illuminated spot on the reflector is assumed to be circular, and a simple model for the mutual intensity function of the reflected field near the spot is used to supply boundary values for integral propagator calculations of the mutual intensity at arbitrary distances. The numerical evaluation of the multiple-integral propagator is made very difficult by the generally rapid oscillations of the integrand over the integration ranges. Methods for overcoming the difficulties are described in this report. Sample calculations are presented, and a listing of a FORTRAN program to perform the integrations is included.

CONTENTS

	Page
1. INTRODUCTION	5
2. PROBLEM FORMULATION	7
3. CALCULATION OF INTEGRAL	10
4. SAMPLE PROBLEM--IDEALIZED GOODMAN SURFACE	38
5. DISCUSSION	50
ACKNOWLEDGEMENT	52
LITERATURE CITED	53
APPENDIX A.--FORTRAN PROGRAM TO CALCULATE PROPAGATION OF MUTUAL INTENSITY FUNCTION	55
DISTRIBUTION	65

FIGURES

1. Geometry of mutual intensity propagation problem 8
2. Geometry for calculating $J(\underset{\sim}{P}'|\Sigma)$ 13
3. Geometry for integrating over σ for evaluating $J(\underset{\sim}{P}'|\sigma)$ 14
4. $J(\underset{\sim}{P}_1'|\sigma)$ for sample problem 22
5. Intensity versus offset from target axis 23
6. Geometry for calculating central contribution 25
7. Mutual intensity at Goodman surface 39
8. Geometry on observation plane for examining $J_B(\underset{\sim}{P}_1',\underset{\sim}{P}_2')$ 44
9. Mutual intensity versus observation point separation--fixed point at center 44

FIGURES

Page

10. Mutual intensity versus observation point separation--fixed point 1 cm from center 45

11. Mutual intensity versus observation point separation--fixed point 3 cm from center 46

12. Mutual intensity versus observation point separation (real part)--fixed point at center 49

13. Mutual intensity versus observation point separation (real part)--fixed point 1 cm from center 49

14. Mutual intensity versus observation point separation (real part)--fixed point 3 cm from center 50

DTIC
ELECTE
JAN 1 1 1983
S D
B

Accession For
NTIS GRA&I ☑
DTIC TAB ☐
Unannounced ☐
Justification
By
Distribution/
Availability Codes
Dist | Avail and/or Special
A

DTIC COPY INSPECTED 2

1. INTRODUCTION

This report discusses the numerical evaluation of certain types of multiple integrals that arise in the theoretical description of short-range coherent laser sensing systems. This work was part of an effort at the Harry Diamond Laboratories (HDL) to explore the fuzing potential of such sensors, which have promise for significantly increased detection sensitivity compared with conventional direct detection systems and would make Doppler information available to the fuze designer.

A critical problem for the performance evaluation of coherent laser fuzes can be seen from the following basic considerations. When a nearly monochromatic laser beam illuminates a nominally flat target surface at normal incidence, the reflected surfaces of constant phase immediately in front of the target will be nominally planar and replicate the surface roughness features, to the extent that shadowing effects do not complicate the picture. If the roughness features have a scale comparable to the illuminating laser's wavelength--a situation which holds for aircraft skins and the CO_2 laser wavelength--then the variation of phase of the reflected field in a plane immediately in front of the target would be expected to oscillate with amplitude on the order of 2π in a random-looking manner, as the observation point traverses the illuminated region. The reflected field retains the temporal coherence of the transmitter laser, but the spatial coherence is severely degraded. Fortunately, as the reflected wavefront propagates in space toward a receiver system, spatial coherence tends to improve; that is, the spatial coherence within a given receiver aperture increases with the distance between the receiver and the reflector. This improvement is important because coherent detection depends on establishing a phase match in space between the reflected and local oscillator wavefronts in the mixing region at the receiver.

In coherent optical radar applications, the receiver apertures and target-to-receiver distances are such that there is virtually no spatial coherence degradation effect. For fuzing applications, however, target-to-receiver distances are usually relatively small--on the order of 10 m--so that, for practical receiver apertures, spatial coherence degradation effects must be considered. This report describes a computational apparatus for analyzing these effects and presents sample calculations. Many aspects of the computational problem present severe numerical difficulties. Methods of overcoming these difficulties are discussed, and a listing of the FORTRAN source code which carries out the calculations is presented in appendix A.

The problem considered is the numerical calculation of the mutual intensity function of the field reflected from a rough surface at arbitrary distances from the reflector. Specifically, we are interested in the mutual intensity function $J_B(\underset{\sim}{P}_1', \underset{\sim}{P}_2')$ between two points, $\underset{\sim}{P}_1'$ and $\underset{\sim}{P}_2'$, on an observation plane--the plane of the receiver aperture--given the mutual intensity function $J_\sigma(\underset{\sim}{P}_1, \underset{\sim}{P}_2)$ between arbitrary points $(\underset{\sim}{P}_1, \underset{\sim}{P}_2)$ in the illuminated target region, σ. The mutual intensity function, defined precisely below, has the information needed to determine spatial coherence degradation effects in the receiver, and its propagation from the target region can be formulated in terms of Huygens-Fresnel integral propagators.[1] In addition, the effect of the rough surface can be modeled through the specification of the mutual intensity function boundary values in the illuminated target region.

The mutual intensity function is used to describe the coherence and intensity pattern of light in space. In this sense it is a generalization of the familiar concept of intensity. Formally, the mutual intensity is defined between two points, $\underset{\sim}{P}_1$ and $\underset{\sim}{P}_2$, as the long-time average of the product of the complex analytic signal of the field

[1] *M. Born and E. Wolf, Principles of Optics, Ch 10, Pergamon Press (1970).*

at $\underset{\sim}{P}_1$ with the complex conjugate of the analytic signal at $\underset{\sim}{P}_2$, where the analytic signals are evaluated at the same time. A further generalization would be to introduce a time element and define a function being the time average product of the analytic signals at $\underset{\sim}{P}_1$ and $\underset{\sim}{P}_2$ when these signals are observed a set time apart. This function is the well-known mutual coherence function of physical optics. (Neither of these functions preserves any polarization information, which would be a further generalization. In this report, however, we will be exclusively concerned with the mutual intensity function.)

We assume that the mutual intensity function is known on some plane in space (the target plane) and that this plane is parallel to the observation plane. In addition, we assume that the mutual intensity function on the target plane is nonzero only over a circular area, σ, and within σ the function depends only on the distance between the evaluation points. That is, given any two points, $\underset{\sim}{P}_1$ and $\underset{\sim}{P}_2$, on the target plane, the mutual intensity between $\underset{\sim}{P}_1$ and $\underset{\sim}{P}_2$ is zero if either $\underset{\sim}{P}_1$ or $\underset{\sim}{P}_2$ is outside σ; otherwise, $J_\sigma(\underset{\sim}{P}_1,\underset{\sim}{P}_2) = J_\sigma(|\underset{\sim}{P}_1 - \underset{\sim}{P}_2|)$. These assumptions, while somewhat restrictive, still include the important case of a homogeneously rough surface with no preferred direction illuminated by a circular beam of coherent light.

2. PROBLEM FORMULATION

We begin with the general equation for the mutual intensity on an observation plane B. Figure 1 shows the geometry being used. We have[1]

$$J_B(\underset{\sim}{P}_1',\underset{\sim}{P}_2') = \int_\sigma \int_\sigma J_\sigma(\underset{\sim}{P}_1,\underset{\sim}{P}_2)\Lambda_1\Lambda_2^* \frac{e^{ik(s_1-s_2)}}{s_1 s_2}\, d\underset{\sim}{P}_1 d\underset{\sim}{P}_2 \quad . \tag{1}$$

[1] *M. Born and E. Wolf, Principles of Optics, Ch 10, Pergamon Press (1970).*

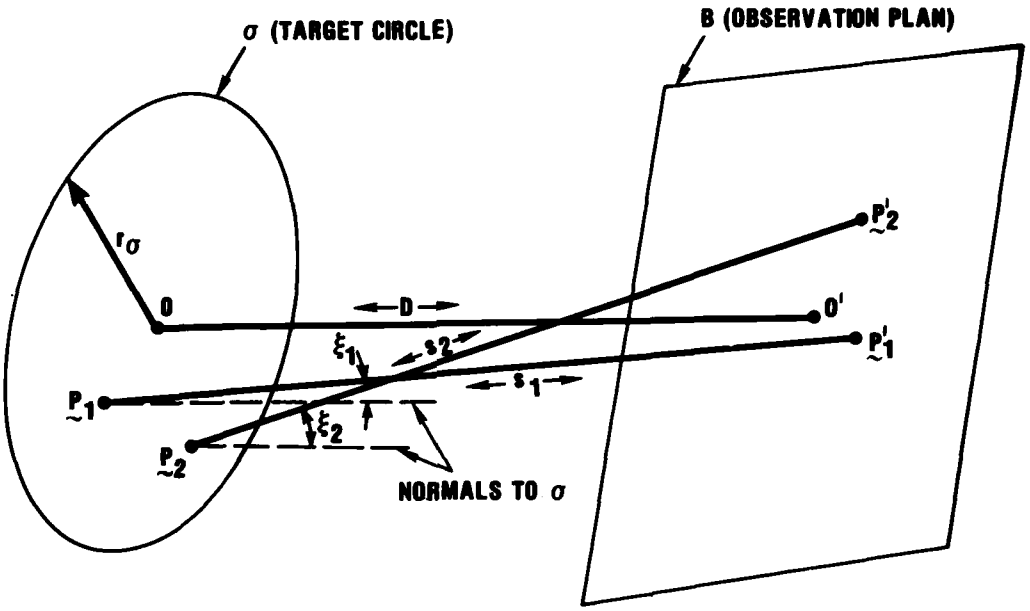

Figure 1. Geometry of mutual intensity propagation problem. (Line OO' is normal to both σ and B.)

In the above, k is the mean wavenumber,* $s_j = |\underset{\sim}{P}_j - \underset{\sim}{P}'_j|$, $i = \sqrt{-1}$, and Λ_j are directionality factors given by

$$\Lambda_j = \frac{i}{\lambda} \cos \xi_j \quad ,$$

where ξ_j is the angle between $(\underset{\sim}{P}_j - \underset{\sim}{P}'_j)$ and the normal to σ, and λ is the wavelength. (The integration is limited to σ because we assume $J_\sigma(\underset{\sim}{P}_1, \underset{\sim}{P}_2)$ is zero outside σ.) From figure 1 we have

$$\Lambda_1 \Lambda_2^* = \left(\frac{kD}{2\pi}\right)^2 \frac{1}{s_1 s_2} \quad , \tag{2}$$

The field is assumed to be nearly monochromatic.

so we obtain

$$J_B(\underset{\sim}{P}_1', \underset{\sim}{P}_2') = \left(\frac{kD}{2\pi}\right)^2 \int_\sigma \int_\sigma J_\sigma(\underset{\sim}{P}_1, \underset{\sim}{P}_2) \frac{e^{ik(s_1 - s_2)}}{s_1^2 s_2^2} d\underset{\sim}{P}_1 d\underset{\sim}{P}_2 \quad . \tag{3}$$

The equations in this form could, in theory, be integrated numerically simply by defining a coordinate system and performing the fourfold nested integration indicated. Typically, however, the wavenumber k i quite large and, unless one is willing to restrict attention to lon range calculations, the quantity $k(s_1 - s_2)$ in the exponential create severe efficiency problems. Additionally, $J_\sigma(\underset{\sim}{P}_1, \underset{\sim}{P}_2)$ is typically finely structured function, with a scale of about 10^{-4} mm. For even moderate-size target σ, this implies excessively large numbers of grid points for straightforward integration.

The above formulation can be simplified within the assumption presented above. Since $J_\sigma(\underset{\sim}{P}_1, \underset{\sim}{P}_2)$ depends only on $|\underset{\sim}{P}_1 - \underset{\sim}{P}_2|$, we can approximately decompose it into a constant term (also termed the residual contribution) and a sum of terms corresponding to varying-size circles of constant-value mutual intensity. That is, we can determine appropriate w_j, a_j, and n such that, for a given error ε,

$$\left| J_\sigma(\underset{\sim}{P}_1, \underset{\sim}{P}_2) - \sum_{j=0}^{n} w_j \hat{J}_\sigma(|\underset{\sim}{P}_1 - \underset{\sim}{P}_2|, a_j) \right| < \varepsilon \quad , \tag{4}$$

where

$$\hat{J}_\sigma(x,a) = \begin{cases} 1 & x \leq a \\ 0 & x > a \end{cases} \quad . \tag{5}$$

The residual term is obtained by setting $a_0 = \infty$. (We note that $J_\sigma(\underset{\sim}{P}_1, \underset{\sim}{P}_2)$ is generally complex, so in general the w_j are complex.) We thus need to consider only the integration

$$\hat{J}_B(\underset{\sim}{P}_1', \underset{\sim}{P}_2') = \left(\frac{kD}{2\pi}\right)^2 \int_\sigma \int_\sigma \hat{J}_\sigma(|\underset{\sim}{P}_1 - \underset{\sim}{P}_2|, a) \frac{e^{ik(s_1 - s_2)}}{s_1^2 s_2^2} d\underset{\sim}{P}_1 d\underset{\sim}{P}_2 \tag{6}$$

for an arbitrary a. This integration will be considered in the next section.

3. CALCULATION OF INTEGRAL

We are now concerned with the integral

$$J_B(\underset{\sim}{P}_1', \underset{\sim}{P}_2') = \left(\frac{kD}{2\pi}\right)^2 \int_\sigma \int_\sigma J_\sigma(|\underset{\sim}{P}_1 - \underset{\sim}{P}_2|, r_c) \frac{e^{ik(s_1 - s_2)}}{s_1^2 s_2^2} d\underset{\sim}{P}_1 d\underset{\sim}{P}_2 \tag{7}$$

(where we have dropped the circumflex notation for J_σ and J_B used in the last section and used r_c, rather than a, as more expressive of a "cutoff radius"). The behavior of $J_\sigma(|\underset{\sim}{P}_1 - \underset{\sim}{P}_2|, r_c)$ can be accounted for by changing the limits of integration

$$J_B(\underset{\sim}{P}_1', \underset{\sim}{P}_2') = \left(\frac{kD}{2\pi}\right)^2 \int_\sigma \int_{\sigma(\underset{\sim}{P}_2)} \frac{e^{ik(s_1 - s_2)}}{s_1^2 s_2^2} d\underset{\sim}{P}_1 d\underset{\sim}{P}_2 \quad , \tag{8}$$

where $\sigma(\underset{\sim}{P}_2)$ is the intersection of σ with a circle of radius r_c centered on $\underset{\sim}{P}_2$. This integral, in turn, splits naturally into two terms:

(1) a "central contribution" term,

$$J_1(\underset{\sim}{P}_1', \underset{\sim}{P}_2') = \left(\frac{kD}{2\pi}\right)^2 \int_{\sigma-\sigma'} \int_{\sigma(\underset{\sim}{P}_2)} \frac{e^{ik(s_1-s_2)}}{s_1^2 s_2^2} \, d\underset{\sim}{P}_1 d\underset{\sim}{P}_2 \quad , \tag{9}$$

where $\sigma - \sigma'$ is the central portion of σ with radius $r_\sigma - r_c$ (where r_σ is the radius of σ) and

(2) an "edge effect" term,

$$J_2(\underset{\sim}{P}_1', \underset{\sim}{P}_2') = \left(\frac{kD}{2\pi}\right)^2 \int_{\sigma'} \int_{\sigma(\underset{\sim}{P}_2)} \frac{e^{ik(s_1-s_2)}}{s_1^2 s_2^2} \, d\underset{\sim}{P}_1 d\underset{\sim}{P}_2 \quad , \tag{10}$$

where σ' is the remaining annulus of breadth r_c on the outside edge of σ. The purpose of this partition of the integral is to isolate the first term, where $\sigma(\underset{\sim}{P}_2)$ does not intersect the edge of σ (and is thus a circle), from the second term, where $\sigma(\underset{\sim}{P}_2)$ is guaranteed to intersect the edge of σ, and hence is a more complicated case. As we shall see later, realistic problems correspond to $r_c \ll r_\sigma$ (except for the residual term), and hence σ' is a relatively small portion of σ.

We note that if $r_c \geq r_\sigma$ the central contribution does not exist; thus, the only contribution is due to the "edge effect," where $\sigma' = \sigma$. Additionally, if $r_c \geq 2r_\sigma$, the intersection of $\sigma(\underset{\sim}{P}_2)$ with σ is σ itself (since $\underset{\sim}{P}_2$ is inside σ), so we obtain in this case

$$J_B(\underset{\sim}{P}_1', \underset{\sim}{P}_2') = J_2(\underset{\sim}{P}_1', \underset{\sim}{P}_2') = \left(\frac{kD}{2\pi}\right)^2 \int_\sigma \int_\sigma \frac{e^{ik(s_1-s_2)}}{s_1^2 s_2^2} \, d\underset{\sim}{P}_1 d\underset{\sim}{P}_2, \; r_c \geq 2r_\sigma \quad . \tag{11}$$

This is the formula for the residual term contribution mentioned in the last section. The integral in this case can be further reduced to the product of two essentially identical integrals as follows.

We have

$$J_B(\underset{\sim}{P}_1', \underset{\sim}{P}_2') = \left(\frac{kD}{2\pi}\right)^2 \int_\sigma \int_\sigma \frac{e^{ik(s_1 - s_2)}}{s_1^2 s_2^2} \, d\underset{\sim}{P}_1 d\underset{\sim}{P}_2, \quad r_c \geq 2r_\sigma$$

$$= \left(\frac{kD}{2\pi}\right)^2 \left(\int_\sigma \frac{e^{iks_1}}{s_1^2} \, d\underset{\sim}{P}_1\right)\left(\int_\sigma \frac{e^{-iks_2}}{s_2^2} \, d\underset{\sim}{P}_2\right) . \tag{12}$$

We now define a function,

$$J(\underset{\sim}{P}' | \Sigma) = \int_\Sigma \frac{e^{iks}}{s^2} \, d\underset{\sim}{P}, \quad s = |\underset{\sim}{P} - \underset{\sim}{P}'| , \tag{13}$$

for arbitrary observation point $\underset{\sim}{P}'$ and arbitrary circle Σ. Figure 2 shows the geometry relevant to the definition of $J(\underset{\sim}{P}' | \Sigma)$. We also define the notational convention that a circumflex over a "prime" point denotes the projection of that point onto the target plane. That is, in a coordinate system with the origin at 0 in figure 2, if

$$\underset{\sim}{P}' = (x', y', D) ,$$

then

$$\hat{\underset{\sim}{P}}' = (x', y', 0) .$$

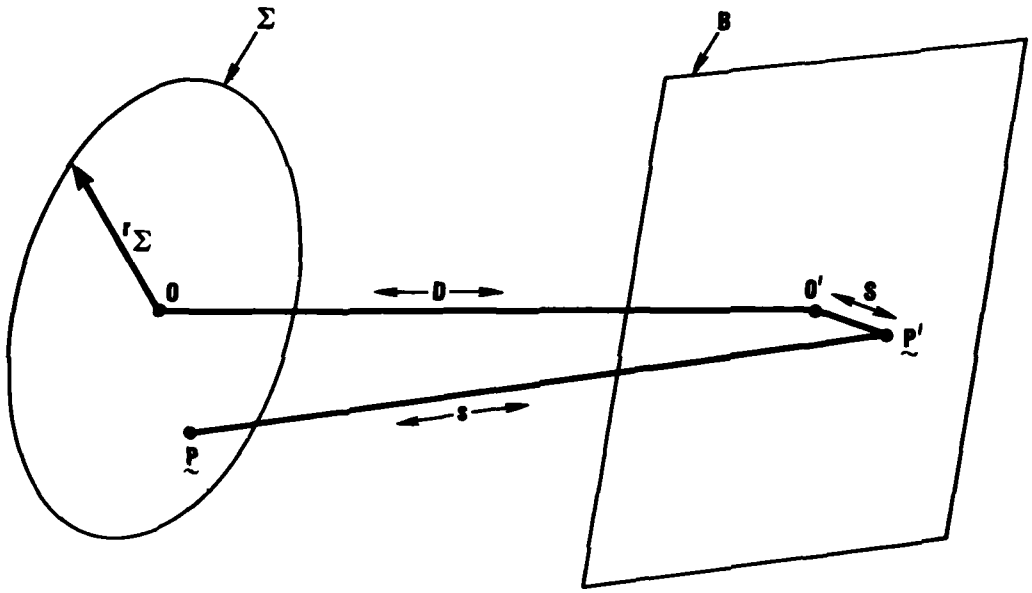

Figure 2. Geometry for calculating $J(\underset{\sim}{P}'|\Sigma)$.

In terms of the $J(\underset{\sim}{P}'|\Sigma)$ function, we have

$$J_B(\underset{\sim}{P}_1', \underset{\sim}{P}_2') = \left(\frac{kD}{2\pi}\right)^2 J(\underset{\sim}{P}_1'|\sigma) J^*(\underset{\sim}{P}_2'|\sigma), \quad r_c \geq 2r_\sigma \quad , \tag{14}$$

where J^* indicates the complex conjugate of J.

We now consider the numerical evaluation of $J(\underset{\sim}{P}'|\sigma)$. We first note that the integrand is constant for all points on any given circle centered at $\hat{\underset{\sim}{P}}'$. This is because s is the slant height of a right circular cone with apex at $\underset{\sim}{P}'$ and a base with a circumference passing through $\underset{\sim}{P}$. Thus, the most natural way to integrate over σ is to use a polar coordinate system centered at $\hat{\underset{\sim}{P}}'$. We show this coordinate system in figure 3, where we have arbitrarily selected the $\theta = 0$ line (using an $r - \theta$ polar coordinate notation) to pass through the center of σ. In this coordinate system, we have $s = \sqrt{D^2 + r^2}$, and the integral becomes

$$J(\underset{\sim}{P}'|\sigma) = \int_{r_o}^{r_\sigma+S} r \frac{e^{ik\sqrt{D^2+r^2}}}{D^2 + r^2} \left[\int_{-\theta_o(r)}^{\theta_o(r)} d\theta\right] dr$$

$$= \int_{r_\sigma}^{r_\sigma+S} 2r\theta_o(r) \frac{e^{ik\sqrt{D^2+r^2}}}{D^2 + r^2} dr \quad , \tag{15}$$

where $\theta_o(r)$ is the angle at which the circle of radius r intersects the boundary of σ, and $r_o = S - r_\sigma$, if $\hat{\underset{\sim}{P}}'$ is outside σ (fig. 3(a)), or $r_o = 0$ if $\hat{\underset{\sim}{P}}'$ is inside σ (fig. 3(b)). The value of $2r\theta_o(r)$ is simply the arc length of the portion of the circle centered at $\hat{\underset{\sim}{P}}'$ of radius r falling inside σ. From simple geometry, assuming that the circles intersect as in figure 3(a), we have

$$\theta_o = \cos^{-1}\left(\frac{r^2 + S^2 - r_\sigma^2}{2Sr}\right) \quad . \tag{16}$$

In figure 3(b), if $r \leq r_\sigma - S$, the circles do not intersect, and we have $\theta_o = \pi$; otherwise, θ_o is still given as above.

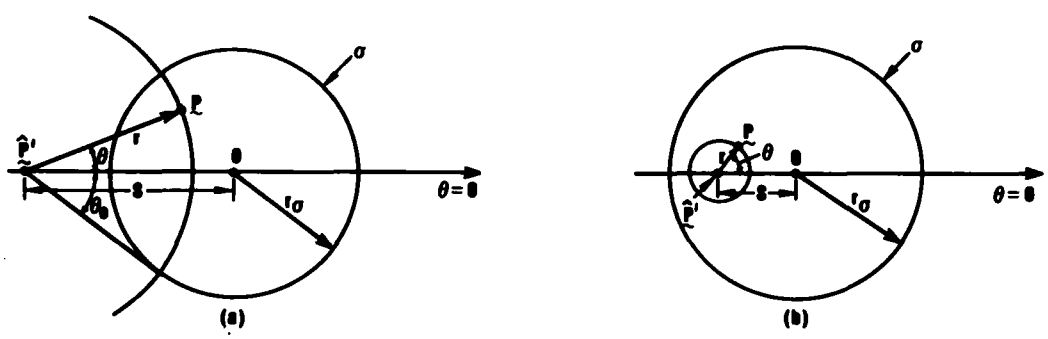

Figure 3. Geometry for integrating over σ for evaluating $J(\underset{\sim}{P}'|\sigma)$: (a) $\hat{\underset{\sim}{P}}'$ falls outside σ. (b) $\hat{\underset{\sim}{P}}'$ falls inside σ; also, $r < r_\sigma - S$.

We thus have two cases. If $\hat{\underset{\sim}{P}}'$ falls outside σ, we have

$$J(\underset{\sim}{P}'|\sigma) = 2\int_{S-r_\sigma}^{S+r_\sigma} r\,\frac{e^{ik\sqrt{D^2+r^2}}}{D^2+r^2}\cos^{-1}\left(\frac{r^2+S^2-r_\sigma^2}{2Sr}\right)dr,\quad S \geq r_\sigma \quad . \tag{17}$$

If $\hat{\underset{\sim}{P}}'$ falls inside σ, we have

$$J(\underset{\sim}{P}'|\sigma) = 2\pi\int_0^{r_\sigma-S} r\,\frac{e^{ik\sqrt{D^2+r^2}}}{D^2+r^2}\,dr$$

$$+\ 2\int_{r_\sigma-S}^{S+r_\sigma} r\,\frac{e^{ik\sqrt{D^2+r^2}}}{D^2+r^2}\cos^{-1}\left(\frac{r^2+S^2-r_\sigma^2}{2Sr}\right)dr, \tag{18}$$

$$S < r_\sigma \quad .$$

The first term of the second case ($S < r_\sigma$) can be integrated in closed form in terms of exponential integrals. We are considering the integral

$$I_1 = 2\pi\int_0^{r_\sigma-S} r\,\frac{e^{ik\sqrt{D^2+r^2}}}{D^2+r^2}\,dr \quad . \tag{19}$$

If we change variables $u = \sqrt{D^2+r^2}$, we obtain

$$I_1 = 2\pi\int_D^{D\sqrt{1+[(r_\sigma-S)/D]^2}} \frac{e^{iku}}{u}\,du \quad . \tag{20}$$

The quantity $\sqrt{1 + [(r_\sigma - S)/D]^2}$ will occur again, so we define

$$\psi = \sqrt{1 + \left(\frac{r_\sigma + S}{D}\right)^2} \quad . \tag{21}$$

We also define

$$\omega = \sqrt{1 + \left(\frac{r_\sigma + S}{D}\right)^2} \quad , \tag{22}$$

which will also be used later. We then have, from the definition[2] of the exponential integral $E_1(z)$,

$$I_1 = 2\pi\left[E_1(-ikD) - E_1(-ikD\psi)\right] \quad . \tag{23}$$

In terms of cosine and sine integrals, Ci(x) and Si(x), we have, from the identity

$$E_1(-ix) = -Ci(x) - iSi(x) + i\,\frac{\pi}{2} \quad , \tag{24}$$

the expression

$$I_1 = 2\pi\left[Ci(kD\psi) - Ci(kD)\right] + i2\pi\left[Si(kD\psi) - Si(kD)\right] \quad . \tag{25}$$

[2] *M. Abramowitz and I. A. Stegun, Handbook of Mathematical Functions with Formulas, Graphs, and Mathematical Tables, NBS Applied Math Series 55 (1970).*

While this expression could be evaluated using any of various methods for calculating the Si and Ci functions, we note that normally kD is very large (on the order of 10^6), so special precautions must be taken. One method well suited to evaluating these functions for large arguments is to express Si(x) and Ci(x) in terms of "auxiliary" functions f(x) and g(x) as[2]

$$\begin{aligned} \mathrm{Si}(x) &= \frac{\pi}{2} - f(x)\cos(x) - g(x)\sin(x) \quad , \\ \mathrm{Ci}(x) &= f(x)\sin(x) - g(x)\cos(x) \quad , \end{aligned} \tag{26}$$

and use asymptotic expansions for f(x) and g(x) for large arguments.

$$\begin{aligned} f(x) &\sim \frac{1}{x}\left(1 - \frac{2!}{x^2} + \frac{4!}{x^4} - \frac{6!}{x^6} + \cdots\right) \\ g(x) &\sim \frac{1}{x^2}\left(1 - \frac{3!}{x^2} + \frac{5!}{x^4} - \frac{7!}{x^6} + \cdots\right) \quad . \end{aligned} \tag{27}$$

For realistic values of kD and $kD\psi$, these expansions converge extremely rapidly; only three or four terms are needed for most calculations. At long ranges, however, when $D \gg r - S$, accuracy may be lost in computing the differences involved in evaluating I_1. If, in the expressions for Si(x) and Ci(x) in terms of f(x), g(x), sin(x), and cos(x), we express ψ as $1 + (\psi - 1)$ in the arguments for sin(x) and cos(x), we can arrive at the expression

$$I_1 = 2\pi e^{ikD}(\alpha + i\beta) \quad , \tag{28}$$

where

$$\begin{aligned} \alpha &= g(kD) + f(kD\psi)\sin[kD(\psi - 1)] - g(kD\psi)\cos[kD(\psi - 1)] \\ \beta &= f(kD) - f(kD\psi)\cos[kD(\psi - 1)] - g(kD\psi)\sin[kD(\psi - 1)] \quad . \end{aligned} \tag{29}$$

---

[2] *M. Abramowitz and I. A. Stegun, Handbook of Mathematical Functions with Formulas, Graphs, and Mathematical Tables, NBS Applied Math Series 55 (1970).*

The factor $\psi - 1$ in the trigonometric functions can be computed at long ranges using the approximation

$$\sqrt{1 + x} \approx 1 + \frac{1}{2} x - \frac{1}{8} x^2 + \frac{1}{16} x^3 \tag{30}$$

to yield

$$\psi - 1 \approx \frac{k(r - S)^2}{2D} \left(1 - \frac{1}{4}\left(\frac{r - S}{D}\right)^2 \left[1 - \frac{1}{2}\left(\frac{r - S}{D}\right)^2\right]\right) . \tag{31}$$

At short ranges, of course, the expression

$$\psi - 1 = \sqrt{1 + \left(\frac{r - S}{D}\right)^2} - 1 \tag{32}$$

should be used.

We now turn attention to the second integral involved in $J(\underset{\sim}{P}'|\sigma)$ (eq (17) and (18)). This integral, in both cases, can be written

$$I_2 = 2 \int_{|S-r_\sigma|}^{S+r_\sigma} r \frac{e^{ik\sqrt{D^2+r^2}}}{D^2 + r^2} \cos^{-1}\left(\frac{r^2 + S^2 - r_\sigma^2}{2Sr}\right) dr . \tag{33}$$

This integral must be evaluated numerically, since no closed-form solution is known. This integral, and several others to be encountered later in this report, will be reduced to a canonical form $\int_L^u f(x)e^{ix}dx$ in order to make use of an efficient numerical integration program

developed at HDL[3] for integrals of this form. The above integral can be reduced to canonical form with the substitution $u = k\sqrt{D^2 + r^2}$, which yields

$$I_2 = 2 \int_{kD\psi}^{kD\omega} \frac{e^{iu}}{u} \cos^{-1}\left[\frac{u^2 - (kD)^2 + (kS)^2 - (kr_\sigma)^2}{2kS\sqrt{u^2 - (kD)^2}}\right] du \quad . \tag{34}$$

At long ranges, the above form for I_2 is unsuited for numerical solution. (Because $\omega - \psi << \psi$, the integration interval is very small compared to the midpoint value of the interval, and severe truncation errors will occur when taking differences.) A solution is to develop a long-range approximate form for I_2. This can be done by expanding the radicals in equations (21) and (22), making a suitable change of variables; that is,

$$\begin{aligned} kD\psi &= kD\sqrt{1 + \left(\frac{r_\sigma - S}{D}\right)^2} \\ &= kD\left[1 + \frac{1}{2}\left(\frac{r_\sigma - S}{D}\right)^2 - \frac{1}{8}\left(\frac{r_\sigma - S}{D}\right)^4 + \frac{1}{16}\left(\frac{r_\sigma - S}{D}\right)^6 \cdots\right] \\ &\approx kD + \frac{k}{2D}(r_\sigma - S)^2\left(1 - \frac{1}{4}\left(\frac{r_\sigma - S}{D}\right)^2\left[1 - \frac{1}{2}\left(\frac{r_\sigma - S}{D}\right)^2\right]\right), \end{aligned} \tag{35}$$

$$D >> |r_\sigma - S| \quad ,$$

[3] *Theodore H. Hopp, A Routine for Numerical Evaluation of Integrals with Oscillation Behavior, Proceedings, 1979 Army Numerical Analysis and Computers Conference, El Paso, TX (1979).*

and

$$kD\omega = kD\sqrt{1 + \left(\frac{r_\sigma + S}{D}\right)^2}$$

$$\approx kD + \frac{k}{2D}\left(r_\sigma + S\right)^2\left(1 - \left[\frac{1}{4}\left(\frac{r_\sigma + S}{D}\right)^2 1 - \frac{1}{2}\left(\frac{r_\sigma + S}{D}\right)^2\right]\right), \tag{36}$$

$$D \gg r_\sigma + S \quad .$$

Changing variables $v = u - kD$, we obtain

$$I_2 \approx 2e^{ikD}\int_{v_L}^{v_H} \frac{e^{iv}}{v + kD} \cos^{-1}\left[\frac{v^2 + 2kDv + (kS)^2 - \left(kr_\sigma\right)^2}{2kS\sqrt{v^2 + 2kDv}}\right] dv, \tag{37}$$

$$D \gg r_\sigma + S \quad ,$$

where

$$v_L = \frac{k\left(r_\sigma - S\right)^2}{2D}\left(1 - \frac{1}{4}\left(\frac{r_\sigma - S}{D}\right)^2 \left[1 - \frac{1}{2}\left(\frac{r_\sigma - S}{D}\right)^2\right]\right)$$

and

$$v_H = \frac{k\left(r_\sigma + S\right)^2}{2D}\left(1 - \frac{1}{4}\left(\frac{r_\sigma + S}{D}\right)^2 \left[1 - \frac{1}{2}\left(\frac{r_\sigma + S}{D}\right)^2\right]\right) \quad . \tag{38}$$

To recapitulate, we now have expressed the function $J(\underset{\sim}{P}'|\sigma)$, for arbitrary $\underset{\sim}{P}'$ and circle σ, as the sum of two integrals, I_1 and I_2. I_1

can be evaluated using asymptotic expansions of the exponential integral $E_1(z)$, and I_2 has been expressed in canonical form for numerical evaluation for both the general case and the long-range case.

Having established how to evaluate $J(\underset{\sim}{P}'|\sigma)$, we can now return to the original problem of calculating $J_B(\underset{\sim}{P}_1',\underset{\sim}{P}_2')$. We have (eq (8) to (10))

$$J_B(\underset{\sim}{P}_1',\underset{\sim}{P}_2') = J_1(\underset{\sim}{P}_1',\underset{\sim}{P}_2') + J_2(\underset{\sim}{P}_1',\underset{\sim}{P}_2') \quad , \tag{39}$$

which reduces to

$$J_B(\underset{\sim}{P}_1',\underset{\sim}{P}_2') = J_2(\underset{\sim}{P}_1',\underset{\sim}{P}_2') = \left(\frac{kD}{2\pi}\right)^2 J(\underset{\sim}{P}_1'|\sigma)\ J^*(\underset{\sim}{P}_2'|\sigma) \tag{40}$$

for $r_c \geq 2r_\sigma$. So far we have not considered how to evaluate $J_2(\underset{\sim}{P}_1',\underset{\sim}{P}_2')$ when $r_c < 2r_\sigma$ or how to evaluate $J_1(\underset{\sim}{P}_1',\underset{\sim}{P}_2')$ at all. Evaluating $J_2(\underset{\sim}{P}_1',\underset{\sim}{P}_2')$ for $r_c < 2r_\sigma$ will not be considered in this report. As mentioned before, for realistic problems, unless the residual contribution is being considered (in which case $r_c \geq 2r_\sigma$), we always have $r_c << r_\sigma$. Since in this case the area of σ' is very small compared to the area of σ, $J_2(\underset{\sim}{P}_1',\underset{\sim}{P}_2')$, being an integral over σ', makes a negligible contribution to $J_B(\underset{\sim}{P}_1',\underset{\sim}{P}_2')$. Before proceeding with the investigation of $J_1(\underset{\sim}{P}_1',\underset{\sim}{P}_2')$, we will illustrate by way of an example the calculations we are now able to perform.

If we consider a target, σ, which is perfectly smooth (i.e., an optically flat mirror), illuminated uniformly by coherent monochromatic

light, the mutual intensity at the target is everywhere a real constant. For simplicity, we will assume this constant to be unity. The mutual intensity at an observation plane parallel to this mirror is precisely $J_B(\underset{\sim}{P}_1', \underset{\sim}{P}_2')$ with $r_c = \infty$ (i.e., the residual contribution). We note that when $\underset{\sim}{P}_1' = \underset{\sim}{P}_2'$, we have

$$J_B(\underset{\sim}{P}_1', \underset{\sim}{P}_1') = \left(\frac{kD}{2\pi}\right)^2 \left|J(\underset{\sim}{P}_1' | \sigma)\right|^2 \quad , \tag{41}$$

which, from the definition of mutual intensity, is the (real) intensity at $\underset{\sim}{P}_1'$. Further, $J_B(\underset{\sim}{P}_1', \underset{\sim}{P}_1')$ can be interpreted as the normalized diffraction pattern from a circular aperture σ. Sample calculations were performed for $J(\underset{\sim}{P}_1' | \sigma)$ for D = 10 m, r_σ = 0.05, λ = 10.6 μm, and for S ranging from 0 to 0.1 m. This choice of parameters places $\underset{\sim}{P}_1'$ well into the near-field region of σ. Plots of $J(\underset{\sim}{P}_1' | \sigma)$ and of $J_B(\underset{\sim}{P}_1', \underset{\sim}{P}_1')$ are shown in figures 4 and 5. (The code used to generate these plots was checked by moving $\underset{\sim}{P}_1'$ to the far-field region of σ to verify the expected Fraunhoeffer diffraction pattern.)

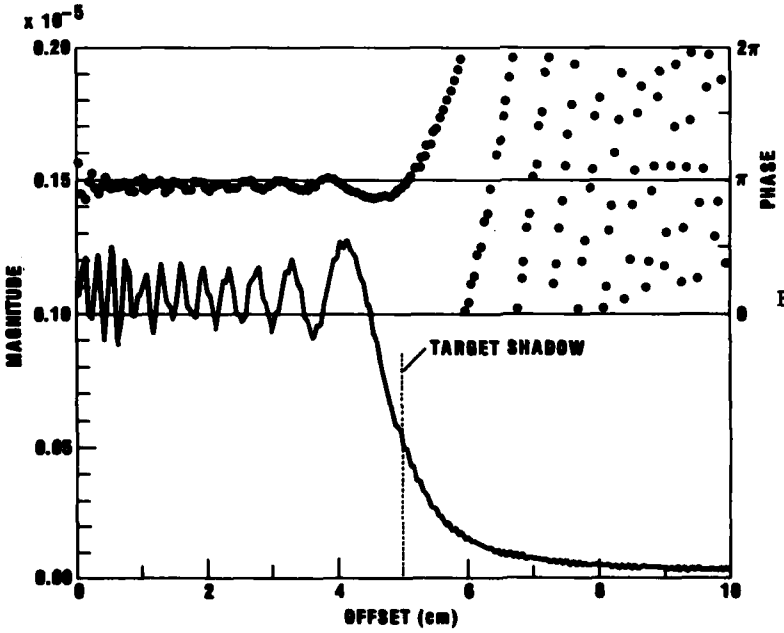

Figure 4. $J(\underset{\sim}{P}_1' | \sigma)$ for sample problem.

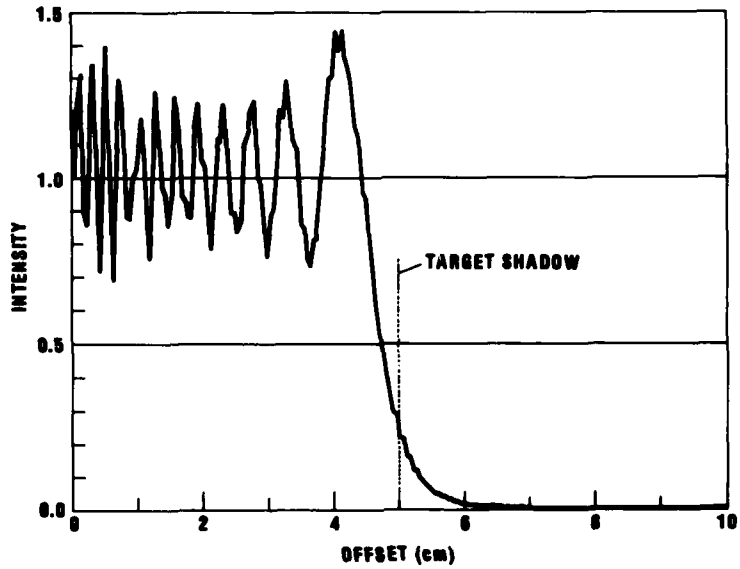

Figure 5. Intensity versus offset from target axis.

We now return to the problem of calculating $J_1(\underset{\sim}{P}_1', \underset{\sim}{P}_2')$. Recall that $J_1(\underset{\sim}{P}_1', \underset{\sim}{P}_2')$ is given by (eq (9))

$$J_1(\underset{\sim}{P}_1', \underset{\sim}{P}_2') = \left(\frac{kD}{2\pi}\right)^2 \int_{\sigma-\sigma'} \int_{\sigma(\underset{\sim}{P}_2)} \frac{e^{ik(s_1-s_2)}}{s_1^2 s_2^2} \, d\underset{\sim}{P}_1 d\underset{\sim}{P}_2 \quad , \tag{42}$$

which can be written

$$J_1(\underset{\sim}{P}_1', \underset{\sim}{P}_2') = \left(\frac{kD}{2\pi}\right)^2 \int_{\sigma-\sigma'} \frac{e^{-iks_2}}{s_2^2} \left[\int_{\sigma(\underset{\sim}{P}_2)} \frac{e^{iks_1}}{s_1^2} \, d\underset{\sim}{P}_1 \right] d\underset{\sim}{P}_2 \quad . \tag{43}$$

But we note that the function $J(\underset{\sim}{P}'|\sigma)$ can be introduced, since $\sigma(\underset{\sim}{P}_2)$ is a circle. We have

$$J[\underset{\sim}{P}_1' | \sigma(\underset{\sim}{P}_2)] = \int_{\sigma(\underset{\sim}{P}_2)} \frac{e^{iks_1}}{s_1^2} \, d\underset{\sim}{P}_1 \quad , \tag{44}$$

so

$$J_1(\underset{\sim}{P}_1', \underset{\sim}{P}_2') = \left(\frac{kD}{2\pi}\right)^2 \int_{\sigma-\sigma'} J[\underset{\sim}{P}_1' | \sigma(\underset{\sim}{P}_2)] \frac{e^{-iks_2}}{s_2^2} \, d\underset{\sim}{P}_2 \quad . \tag{45}$$

From its definition, $J[\underset{\sim}{P}_1' | \sigma(\underset{\sim}{P}_2)]$ has circular symmetry about $\underset{\sim}{P}_2$. Equivalently, it has circular symmetry about $\hat{\underset{\sim}{P}}_1'$. Since the major work in evaluating the integrand of $J_1(\underset{\sim}{P}_1', \underset{\sim}{P}_2')$ is in evaluating $J[\underset{\sim}{P}_1' | \sigma(\underset{\sim}{P}_2)]$, it is natural to express the integral in polar coordinates about $\hat{\underset{\sim}{P}}_1'$. The geometry involved is shown in figure 6. We define the $\theta = 0$ axis as passing through $\hat{\underset{\sim}{P}}_1'$ and $\hat{\underset{\sim}{P}}_2'$. Defining the aperture function

$$u(r,\theta;\sigma) = \begin{cases} 1 \text{ if } (r,\theta) \text{ is inside } \sigma \\ 0 \text{ otherwise} \end{cases} \quad , \tag{46}$$

we obtain

$$J(\underset{\sim}{P}_1', \underset{\sim}{P}_2') = \left(\frac{kD}{2\pi}\right)^2 \int_{r_0}^{R_1+(r_\sigma - r_c)} r J[\underset{\sim}{P}_1' | \sigma(\underset{\sim}{P}_2)] \left[\int_0^{2\pi} u(r,\theta;\sigma - \sigma') \frac{e^{-iks_2}}{s_2^2} \, d\theta\right] dr \quad , \tag{47}$$

where R_1, from figure 6, is the distance from $\hat{\underset{\sim}{P}}_1'$ to the center of $\sigma - \sigma'$ and r_0 is given by

$$r_0 = \begin{cases} 0 \text{ if } \hat{\underset{\sim}{P}}_1' \text{ is inside } \sigma - \sigma' \\ R_1 - \left(r_\sigma - r_c\right) \text{ if } \hat{\underset{\sim}{P}}_1' \text{ is outside } \sigma - \sigma' \end{cases} . \tag{48}$$

Also from figure 6, and the law of cosines, we have

$$s_2 = \sqrt{D^2 + r^2 + d^2 - 2rd \cos \theta} \quad , \tag{49}$$

where d is the distance between $\hat{\underset{\sim}{P}}_1'$ and $\hat{\underset{\sim}{P}}_2'$.

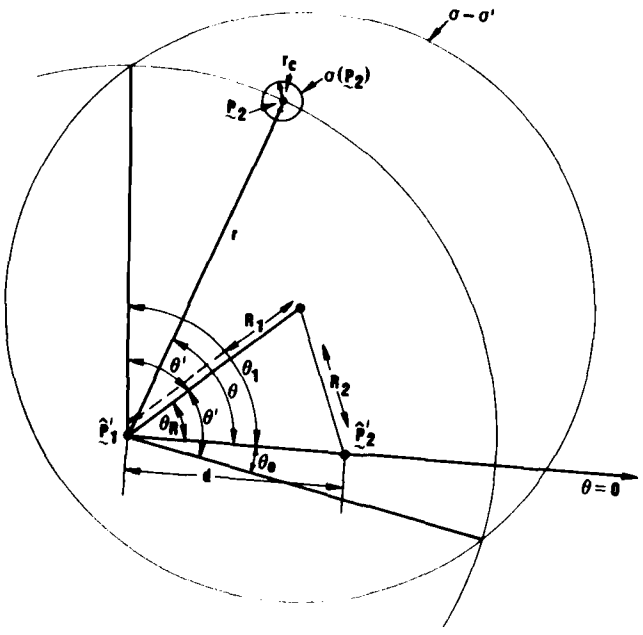

Figure 6. Geometry for calculating central contribution.

When $r \leq (r_\sigma - r_c) - R_1$, $u(r,\theta;\sigma - \sigma') = 1$ for all values of θ. This occurs only when $\hat{\underset{\sim}{P}}_1'$ is inside $\sigma - \sigma'$ (as shown in fig. 6). When $(r_\sigma - r_c) - R_1 < r \leq R_1 + (r_\sigma - r_c)$, there is a pair of values (θ_0, θ_1) such that $u(r,\theta;\sigma - \sigma') = 1$ only when $\theta_0 \leq \theta \leq \theta_1$ (also shown in fig. 6). From the diagram we see that there is a θ' such that $\theta_0 = \theta_R - \theta'$ and $\theta_1 = \theta_R + \theta'$. If $\hat{\underset{\sim}{P}}_1'$ is at $(x_1', y_1', 0)$ and $\hat{\underset{\sim}{P}}_2'$ is at $(x_2', y_2', 0)$, with the origin at the center of σ, we have from simple geometry

$$
\begin{aligned}
R_1 &= \sqrt{x_1'^2 + y_1'^2} \quad , \\
R_2 &= \sqrt{x_2'^2 + y_2'^2} \quad , \\
d &= \sqrt{(x_1' - x_2')^2 + (y_1' - y_2')^2} \quad , \\
\theta_R &= \cos^{-1}\left(\frac{R_1^2 + d^2 - R_2^2}{2R_1 d}\right) \quad ,
\end{aligned}
\tag{50}
$$

and

$$
\theta' = \cos^{-1}\left(\frac{r^2 + R_1^2 - (r_\sigma - r_c)^2}{2rR_1}\right) \quad .
$$

When $\hat{\underset{\sim}{P}}_1'$ falls outside $\sigma - \sigma'$ $(R_1 \geq r_\sigma - r_c)$ we have

$$J_1(\underset{\sim}{P}_1', \underset{\sim}{P}_2') = \left(\frac{kD}{2\pi}\right)^2 \int_{R_1-(r_\sigma-r_c)}^{R_1+(r_\sigma-r_c)} rJ[\underset{\sim}{P}_1' | \sigma(\underset{\sim}{P}_2)] \left[\int_{\theta_R-\theta'}^{\theta_R+\theta'} \frac{e^{-iks_2}}{s_2^2} d\theta \right] dr \quad . \tag{51}$$

When $\hat{\underset{\sim}{P}}_1'$ falls inside $\sigma - \sigma'$ $(R_1 < r_\sigma - r_c)$, we have

$$\begin{aligned} J_1(\underset{\sim}{P}_1', \underset{\sim}{P}_2') = \left(\frac{kD}{2\pi}\right)^2 & \int_0^{(r_\sigma-r_c)-R_1} rJ[\underset{\sim}{P}_1' | \sigma(\underset{\sim}{P}_2)] \left[\int_0^{2\pi} \frac{e^{-iks_2}}{s_2^2} d\theta \right] dr \\ & + \left(\frac{kD}{2\pi}\right)^2 \int_{(r_\sigma-r_c)-R_1}^{(r_\sigma-r_c)+R_1} rJ\,[\underset{\sim}{P}_1' | \sigma(\underset{\sim}{P}_2)] \left[\int_{\theta_R-\theta'}^{\theta_R+\theta'} \frac{e^{-iks_2}}{s_2^2} d\theta \right] dr \quad . \end{aligned} \tag{52}$$

At this point we have two integrals to evaluate to obtain $J_1(\underset{\sim}{P}_1', \underset{\sim}{P}_2')$ and thence $J_B(\underset{\sim}{P}_1', \underset{\sim}{P}_2')$, namely, the outer integral of equations (51) and (52), which is an integration in r, and the inner integral in θ, which has the two forms

$$\int_0^{2\pi} \frac{e^{-iks_2}}{s_2^2} d\theta = \left[\int_0^{2\pi} \frac{e^{iks_2}}{s_2^2} d\theta \right]^* \tag{53}$$

and

$$\int_{\theta_R-\theta'}^{\theta_R+\theta'} \frac{e^{-iks_2}}{s_2^2}\, d\theta = \left[\int_{\theta_R-\theta'}^{\theta_R+\theta'} \frac{e^{iks_2}}{s_2^2}\, d\theta\right]^* \quad . \tag{54}$$

These forms will be considered next.

In order to reduce the integrals in θ to canonical forms, we would like to make the change of variables $u = ks_2$. However, since $s_2 = \sqrt{D^2 + r^2 + d^2 - 2rd \cos\theta}$, we must restrict the range of θ (say, to $0 \leq \theta \leq \pi$) for the change of variables to be valid. Thus, each of the above forms must be modified to meet this condition on the range of integration. Because of the nature of $\cos\theta$, the first form can be easily changed:

$$\int_0^{2\pi} \frac{e^{iks_2}}{s_2^2}\, d\theta = 2\int_0^{\pi} \frac{e^{iks_2}}{s_2^2}\, d\theta \quad . \tag{55}$$

This leaves the second form to consider:

$$\int_{\theta_R-\theta'}^{\theta_R+\theta'} \frac{e^{iks_2}}{s_2^2}\, d\theta \quad .$$

From the equations (50) for θ_R and θ', we have

$$0 \leq \theta_R, \theta' \leq \pi \quad ;$$

thus,

$$-\pi \leq \theta_R - \theta' \leq \pi \quad ,$$

and

$$0 \leq \theta_R + \theta' \leq 2\pi \quad .$$

We identify four cases:

(1) $\theta_R - \theta' \geq 0, \quad \theta_R + \theta' \leq \pi \quad .$

In this case the variable transformation in question has a single-valued inverse on the range of integration.

(2) $\theta_R - \theta' < 0, \quad \theta_R + \theta' \leq \pi \quad .$

In this case the integration can be treated as follows:

$$\int_{\theta_R-\theta'}^{\theta_R+\theta'} \ldots \, d\theta = \int_{\theta_R-\theta'}^{0} \ldots \, d\theta + \int_{0}^{\theta_R+\theta'} \ldots \, d\theta$$

$$= \int_{0}^{-(\theta_R-\theta')} \ldots \, d\theta + \int_{0}^{\theta_R+\theta'} \ldots \, d\theta \tag{56}$$

$$= 2\int_{0}^{\theta'-\theta_R} \ldots \, d\theta + \int_{\theta'-\theta_R}^{\theta'+\theta_R} \ldots \, d\theta \quad .$$

The last step is taken to avoid integrating over $[0,\theta']$ twice.

(3) $\theta_R - \theta' \geq 0, \quad \theta_R + \theta' > \pi$.

The integration is treated as follows:

$$\int_{\theta_R}^{\theta_R+\theta'} \ldots \, d\theta = \int_{\theta_R-\theta'}^{\pi} \ldots \, d\theta + \int_{\pi}^{\theta_R+\theta'} \ldots \, d\theta \, ,$$

$$= \int_{\theta_R-\theta'}^{\pi} \ldots \, d\theta - \int_{\pi}^{2\pi-(\theta_R+\theta')} \ldots \, d\theta \, ,$$

(using the substitution $\theta \leftarrow 2\pi - \theta$)

$$= \int_{\theta_R-\theta'}^{\pi} \ldots \, d\theta + \int_{2\pi-(\theta_R+\theta')}^{\pi} \ldots \, d\theta \, , \tag{57}$$

$$= \int_{\theta_R-\theta'}^{2\pi-(\theta_R+\theta')} \ldots \, d\theta + 2\int_{2\pi-(\theta_R+\theta')}^{\pi} \ldots \, d\theta \quad . \tag{57}$$

The last step follows from observing that since $\theta_R \leq \pi$, $\theta_R - \theta' < 2\pi - (\theta_R + \theta')$.

(4) $\theta_R - \theta' < 0, \quad \theta_R + \theta' > \pi$.

The integration is treated as follows:

$$\int_{\theta_R-\theta'}^{\theta_R+\theta'} \ldots \, d\theta = \int_{\theta_R-\theta'}^{0} \ldots \, d\theta + \int_{0}^{\pi} \ldots \, d\theta + \int_{\pi}^{\theta_R+\theta'} \ldots \, d\theta$$

$$= \int_{0}^{\theta'-\theta_R} \ldots \, d\theta + \int_{0}^{\pi} \ldots \, d\theta + \int_{2\pi-(\theta_R+\theta')}^{\pi} \ldots \, d\theta \tag{58}$$

$$= 2\int_{0}^{\theta'-\theta_R} \ldots \, d\theta + \int_{\theta'-\theta_R}^{2\pi-(\theta_R+\theta')} \ldots \, d\theta$$

$$+ 2\int_{2\pi-(\theta_R+\theta')}^{\pi} \ldots \, d\theta \quad .$$

In the last step, since $\theta' \leq \pi$, we are assured that $\theta' - \theta_R < 2\pi - (\theta_R + \theta')$. In all cases, the integral in θ can be broken down into a sum of integrals, each of which is over an interval $[\theta_L, \theta_U]$, where

$0 \leq \theta_L \leq \theta_U \leq \pi$ and hence $u = ks_2$ is uniquely invertible on each such interval. We can then perform the change of variable to reduce all these integrals to canonical form. We have

$$u = ks_2 = k\sqrt{D^2 + r^2 + d^2 - 2rd \cos \theta} \quad , \tag{59}$$

yielding

$$d\theta = \frac{2udu}{k^2\sqrt{4rd^2 - \left[D^2 + r^2 + d^2 - (u/k)^2\right]^2}} \quad , \tag{60}$$

$$u\big|_{\theta=\theta_L} = kD\sqrt{1 + \left(\frac{r - d}{D}\right)^2 + \frac{2rd}{D^2}\left(1 - \cos \theta_L\right)} \quad , \tag{61}$$

$$u\big|_{\theta=\theta_U} = kD\sqrt{1 + \left(\frac{r + d}{D}\right)^2 - \frac{2rd}{D^2}\left(1 + \cos \theta_U\right)} \quad . \tag{62}$$

If we define the quantities

$$A = kD\sqrt{1 + \left(\frac{r - d}{D}\right)^2} \quad , \tag{63}$$

$$B = kD\sqrt{1 + \left(\frac{r + d}{D}\right)^2} \quad , \tag{64}$$

we have

$$d\theta = \frac{2udu}{\sqrt{\left(u^2 - A^2\right)\left(B^2 - u^2\right)}} \quad , \tag{65}$$

$$u\big|_{\theta=\theta_L} = \sqrt{A^2 + 2rdk^2\left(1 - \cos\ \theta_L\right)} \quad , \tag{66}$$

$$u\big|_{\theta=\theta_U} = \sqrt{B^2 - 2rdk^2\left(1 + \cos\ \theta_U\right)} \quad . \tag{67}$$

Finally, we obtain

$$\int_{\theta_L}^{\theta_U} \frac{e^{iks_2}}{s_2^2}\, d\theta = 2k^2 \int_{\sqrt{A^2+2rdk^2\left(1-\cos\theta_L\right)}}^{\sqrt{B^2-2rdk^2\left(1+\cos\theta_U\right)}} e^{iu} \frac{du}{u\sqrt{\left(u^2 - A^2\right)\left(B^2 - u^2\right)}} \quad . \tag{68}$$

As in the integration for $J_2\left(\underset{\sim}{P}_1', \underset{\sim}{P}_2'\right)$, when $D >> r + d$ numerical problems arise because the interval of integration is small compared to the

location of the interval. In the integral, we have two differences of large numbers to consider, namely, u - A and B - u. If we perform the change of variable $x \leftarrow u - A$, we obtain

$$\int_{\theta_L}^{\theta_U} \frac{e^{iks_2}}{s_2^2}\, d\theta = 2k^2 e^{iA} \int_{\sqrt{A^2+2rdk^2(1-\cos\theta_L)} - A}^{\sqrt{B^2-2rdk^2(1+\cos\theta_U)} - A} \tag{69}$$

$$\times \frac{e^{ix}\, dx}{(x + A)\sqrt{x(B - A - x)(x + 2A)(x + A + B)}} \; .$$

Now all the differences between large numbers can be calculated beforehand. We are concerned with the quantities

$$x_L = \sqrt{A^2 + 2rdk^2(1 - \cos\theta_L)} - A \; ,$$

$$x_U = \sqrt{B^2 - 2rdk^2(1 + \cos\theta_U)} - A \; , \tag{70}$$

and

$$B - A \; .$$

Substituting for A and B, and using the expansion

$$\sqrt{1 + x} \approx 1 + \frac{1}{2} x - \frac{1}{8} x^2 + \frac{1}{16} x^3 \quad , \tag{71}$$

we obtain

$$x_L \approx \frac{krd(1 - \cos \theta_L)}{D} \left(1 - \frac{1}{2} \frac{(r - d)^2 + rd(1 - \cos \theta_L)}{D^2} \left[1 - \frac{(r - d)^2 + rd(1 - \cos \theta_L)}{D^2}\right] - \frac{(r - d)^2 \left[(r - d)^2 + 2rd(1 - \cos \theta_L)\right]}{8D^4}\right) \quad . \tag{72}$$

$$x_U \approx \frac{krd(1 - \cos \theta_U)}{D} \left(1 - \frac{1}{2} \frac{(r - d)^2 + rd(1 - \cos \theta_U)}{D^2} \left[1 - \frac{(r - d)^2 + rd(1 - \cos \theta_U)}{D^2}\right] - \frac{(r - d)^2\left[(r - d)^2 + 2rd(1 - \cos \theta_U)\right]}{8D^4}\right) \quad , \tag{73}$$

and

$$B - A \approx \frac{2krd}{D}\left[1 - \frac{1}{2} \frac{r^2 + d^2}{D^2} \left(1 - \frac{r^2 + d^2}{D^2}\right) - \frac{(r^2 - d^2)^2}{8D^4}\right] \quad . \tag{74}$$

The substitution $x \leftarrow u - A$ works well unless the entire interval of integration is very close to the singularity at B. This happens when

both $|\cos\theta_U - \cos\theta_L| << 1$ and $|1 + \cos\theta_U| << 1$. In this case, we are better off using the substitution $y \leftarrow u - B$. This yields

$$\int_{\theta_L}^{\theta_U} \frac{e^{iks_2}}{s_2^2}\, d\theta = 2k^2\, e^{iB} \int_{\sqrt{A^2+2rdk^2(1-\cos\theta_L)}-B}^{\sqrt{B^2-2rdk^2(1+\cos\theta_U)}-B} \tag{75}$$

$$\times \frac{e^{iy}\, dy}{(y + B)\sqrt{(B - A + y)(-y)(y + B + A)(y + 2B)}} \; .$$

We still need to calculate $B - A$, as above, but the expressions for the limits of integration have changed. We now need the values

$$y_L = \sqrt{A^2 + 2rdk^2(1 - \cos\theta_L)} - B \tag{76}$$

and

$$y_U = \sqrt{B^2 - 2rdk^2(1 + \cos\theta_U)} - B \; . \tag{77}$$

Using the same expansion for $\sqrt{1 + x}$, we obtain

$$y_L \approx -\frac{krd(1 + \cos\theta_L)}{D}\left(1 - \frac{1}{2}\frac{(r + d)^2 - rd(1 + \cos\theta_L)}{D^2}\right.$$

$$\times \left[1 - \frac{(r + d)^2 - rd(1 + \cos\theta_L)}{D^2}\right] \tag{78}$$

$$\left. - \frac{(r + d)^2[(r + d)^2 - 2rd(1 + \cos\theta_L)]}{8D^4}\right) \; ,$$

and

$$y_U \approx -\frac{krd(1 + \cos\theta_U)}{D}\left(1 - \frac{1}{2}\frac{(r + d)^2 - rd(1 + \cos\theta_U)}{D^2}\right.$$

$$\times\left[1 - \frac{(r + d)^2 - rd(1 + \cos\theta_U)}{D^2}\right] \tag{79}$$

$$\left. - \frac{(r + d)^2[(r + d)^2 - 2rd(1 + \cos\theta_U)]}{8D^4}\right) .$$

This second substitution, in turn, works well unless the interval of integration is near the singularity at A. This happens only when $|\cos\theta_U - \cos\theta_L| << 1$ and $|1 - \cos\theta_L| << 1$. Since the interval of integration cannot be entirely located near A and entirely located near B at the same time, one or the other of the above substitutions can be used for any problem. We will use the first substitution, $x \leftarrow u - A$, unless $\cos\theta_L < 0$. In that event we will use the substitution $y \leftarrow u - B$, since $|1 - \cos\theta_L| << 1$ cannot hold.

At this point we have specified how to do all the calculations for $J_1(\underset{\sim}{P}_1', \underset{\sim}{P}_2')$, except the integral in r. The integrands in this case cannot be expressed in the canonical form $e^{ix}f(x)$ in any useful way, so another method of integration is needed. As will be shown in the next section, the behavior of the integrand in this integral is quite varied in character, depending strongly on the separation of the observation points $\underset{\sim}{P}_1'$ and $\underset{\sim}{P}_2'$. Thus, the number of points at which will be necessary to evaluate the integrand cannot be predicted we Rather than using a fixed Gaussian quadrature scheme where all the work done at one

level of approximation is useless at the next level of accuracy, it would be more sensible to use an integration scheme that makes use of all previous work when trying to increase the precision of the integration. One of the best such schemes is an adaptive Gaussian scheme modified to force all points previously used to be included at the next level of precision.[4] Since such a routine has already been developed,[5] we will not elaborate on it here. Rather, we will proceed to describe the results of calculations for a sample problem.

4. SAMPLE PROBLEM--IDEALIZED GOODMAN SURFACE

In the previous section we described how to evaluate the mutual intensity between two points on an observation plane when the mutual intensity of the reflected radiation at the target plane is given by

$$J_\sigma(\underset{\sim}{P}_1,\underset{\sim}{P}_2) = \hat{J}_\sigma(|\underset{\sim}{P}_1 - \underset{\sim}{P}_2|, r_c) = \begin{cases} 1 \text{ if } |\underset{\sim}{P}_1 - \underset{\sim}{P}_2| < r_c \text{ and} \\ \qquad \underset{\sim}{P}_1 \text{ and } \underset{\sim}{P}_2 \text{ are inside } \sigma \\ 0 \text{ otherwise} \end{cases} \tag{80}$$

for an arbitrary cutoff radius r_c. The justification for considering such a simple model for J_σ was briefly mentioned in section 1. Any J_σ that depends only on the distance between the evaluation points $\underset{\sim}{P}_1$ and $\underset{\sim}{P}_2$ can be approximated arbitrarily well by a finite sum of functions of the above form with various r_c's; moreover, such a J_σ dependence is expected when a flat, homogeneously and isotropically

---

[4] *T. N. L. Patterson, The Optimum Addition of Points to Quadrature Formulae, Math. Comp., 22 (1968), 847-856.*

[5] *T. N. L. Patterson, Algorithm for Automatic Numerical Integration Over a Finite Interval, Algorithm 468 Comm. of the ACM, 16, 11 (November 1973), 694-699.*

rough target is illuminated by a coherent light beam. Further justification for considering the form of equation (80) is furnished by Goodman's recent discussion[6] of a simple physical model of J_σ for flat rough surfaces whose slope distribution is concentrated mainly in a low slope region.

An example of Goodman's predictions for J_σ is shown by the solid curve in figure 7, which assumes uniform reflected intensity of unity at σ; also shown, by dotted lines, is a rough approximation to the predicted J_σ-curve by two functions of the form in equation (80). It is clear from figure 7 that very good approximations of Goodman-surface J_σ's can be obtained by using only a few different values of r_c.

In this section, we apply the results of section 2 to an example, namely, that of a target whose J_σ corresponds to the Goodman surface of figure 7. We approximate J_σ by the dotted step function in figure 7 and calculate $J_B(\underset{\sim}{P}_1', \underset{\sim}{P}_2')$ at an observation plane for various $\underset{\sim}{P}_1', \underset{\sim}{P}_2'$ pairs.

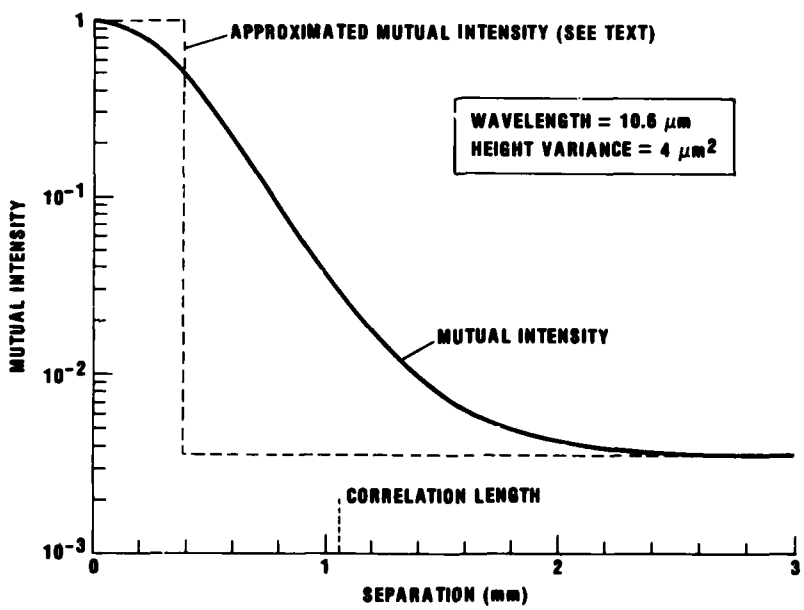

Figure 7. Mutual intensity at Goodman surface.

[6] *J. W. Goodman, Statistical Properties of Laser Speckle Patterns, Laser Speckle and Related Phenomena, Ed., J. C. Dainty, Topics in Applied Physics, 9, Springer-Verlag (1975), 63-68.*

In its simplest form, Goodman's model describes J_σ in terms of the second-order statistics of the surface height variations. Specifically, we have

$$J_G(\underset{\sim}{P}_1, \underset{\sim}{P}_2) = \sqrt{I(\underset{\sim}{P}_1) I(\underset{\sim}{P}_2)} \exp\left(-\sigma_\theta^2 \left[1 - \rho_h(|\underset{\sim}{P}_1 - \underset{\sim}{P}_2|)\right]\right) \quad . \tag{81}$$

In the above, $J_G(\underset{\sim}{P}_1, \underset{\sim}{P}_2)$ is the Goodman model J_σ and $I(\underset{\sim}{P})$ is the reflected intensity at point P. In the exponential, σ_θ^2 is the surface height variance scaled to the effective wavelength, given by

$$\sigma_\theta^2 = [k(1 + \cos \beta)]^2 \sigma^2{}_h \quad , \tag{82}$$

where k is the wave number, β is the angle of illumination relative to the surface normal, and σ_h^2 is the actual variance of the surface height. Finally $\rho_h(x)$ is the normalized surface height autocorrelation function, which, for simplicity, is assumed to be of the form

$$\rho_h(|\underset{\sim}{P}_1 - \underset{\sim}{P}_2|) = \exp\left(- \frac{|\underset{\sim}{P}_1 - \underset{\sim}{P}_2|^2}{r_o^2}\right) \quad , \tag{83}$$

where r_o is the surface roughness correlation length. The distance r_o is the separation at which the surface height correlation reaches a value of 1/e. Figure 7 plots a typical $J_G(\underset{\sim}{P}_1, \underset{\sim}{P}_2)$ versus $|\underset{\sim}{P}_1 - \underset{\sim}{P}_2|$.

The numerical parameter values used to produce figure 7, and which will be used for the sample problem of this section, are as follows:

Wavelength (λ) = 10.6 μm,

Surface height standard deviation (σ_h) = 2 μm, (84)

Angle of illumination (β) = 0,

Surface correlation length (r_o) = 1.06 mm (= 100λ).

These values correspond to a surface that is optically flat over distances on the scale of 100 wavelengths, illuminated perpendicularly by a 10.6-μm laser (e.g., a CO_2 laser), and observed at a distance of 10 m. Hills and valleys on the surface average 2 μm of deviation from the mean surface height. These values yield, for the other quantities used in the Goodman model,

$$\sigma_\theta^2 = 5.6217 \quad ,$$

$$\rho_h(x) = \exp\left(-889{,}996\ x^2\right) \ . \tag{85}$$

For our sample problem we take

$$J_\sigma(\underset{\sim}{P}_1, \underset{\sim}{P}_2) = e^{-\sigma_\theta^2}\ \hat{J}_\sigma(|\underset{\sim}{P}_1 - \underset{\sim}{P}_2|, \infty) + \left(1 - e^{-\sigma_\theta^2}\right) \hat{J}_\sigma(|\underset{\sim}{P}_1 - \underset{\sim}{P}_2|, r_c) \quad , \tag{86}$$

where r_c is chosen as that point separation for which $J_G = \left(1 + e^{-\sigma_\theta^2}\right)/2$; i.e., the separation at which J_G has fallen halfway from its maximum value of unity to its minimum value $e^{-\sigma_\theta^2}$. The desired value of r_c is readily found as

$$r_c = r_o \sqrt{\ln\left[\sigma_\theta^2 / \ln\left(\frac{e^{\sigma_\theta^2} + 1}{2}\right)\right]} \quad , \tag{87}$$

which for the chosen numerical values of the sample problem gives $r_c = 3.83445 \times 10^{-4}$ m. Equation (86) gives the dotted line approximation to J_G shown in figure 7. To complete the specification of our sample problem, we take

$$\begin{aligned} \text{Range (D)} &= 10 \text{ m} \\ \text{Target spot radius } (r_o) &= 0.05 \text{ m} \quad . \end{aligned} \tag{88}$$

(Note that these values are the same as were used for the sample diffraction pattern calculations of the last section.)

The contribution to $J_B(\underset{\sim}{P}_1', \underset{\sim}{P}_2')$ from the first term of equation (86) is

$$e^{-\sigma_\theta^2} \left(\frac{kD}{2\pi}\right)^2 J(\underset{\sim}{P}_1' | \sigma)\, J^*(\underset{\sim}{P}_2' | \sigma)$$

(compare with eq (4) and (40)). We call this part of J_B the residual contribution since it arises from the low dotted plateau in figure 7, which represents the residual phase correlation in the reflected field at σ in the limit of large point separation. The residual phase correlation is physically related to the specular component of reflection from the target. Figure 4 plots the modulus and phase of $J(\underset{\sim}{P}'|\sigma)$ appropriate to our sample problem. The contribution of the second term in equation (86) (which corresponds to the high phase correlation shown by J_G for small point separations) to $J_B(\underset{\sim}{P}_1', \underset{\sim}{P}_2')$ is more difficult to represent since it depends not only on the separation of $\underset{\sim}{P}_1'$ and $\underset{\sim}{P}_2'$, but also on their location within the shadow of σ. (We will denote by $\hat{\sigma}$ the shadow of σ on the observation plane.) We note that $J_B(\underset{\sim}{P}_1', \underset{\sim}{P}_2')$ is invariant to rotation about the center of $\hat{\sigma}$ since the problem is circularly symmetric. We also note that $J_B(\underset{\sim}{P}_1', \underset{\sim}{P}_2')$ is invariant to reflection through the center of $\hat{\sigma}$. Thus, one convenient way of examining $J_B(\underset{\sim}{P}_1', \underset{\sim}{P}_2')$ is to fix one of the points (say, $\underset{\sim}{P}_1'$) at some distance from the center of $\hat{\sigma}$ and move the other point $(\underset{\sim}{P}_2')$ away from $\underset{\sim}{P}_1'$ at various angles from the radius. The geometry of this layout is shown in figure 8.

Figures 9 to 11 show the results of calculations for the sample problem for three positions of the fixed point, $\underset{\sim}{P}_1'$. Figure 9 shows what happens when $\underset{\sim}{P}_1'$ is at the center of $\hat{\sigma}$ $(R_1 = 0)$ and $\underset{\sim}{P}_2'$ is moved away from $\underset{\sim}{P}_1'$. (Since this case is circularly symmetric about $\underset{\sim}{P}_1'$, there is no need to plot what happens at different angles from a radius.) As can be seen, the sharp step function character of the approximated mutual intensity at the target plane (fig. 7) has been spread out substantially, although it is still apparent that the mutual intensity between $\underset{\sim}{P}_1'$ and $\underset{\sim}{P}_2'$ is stronger when the two points are close together.

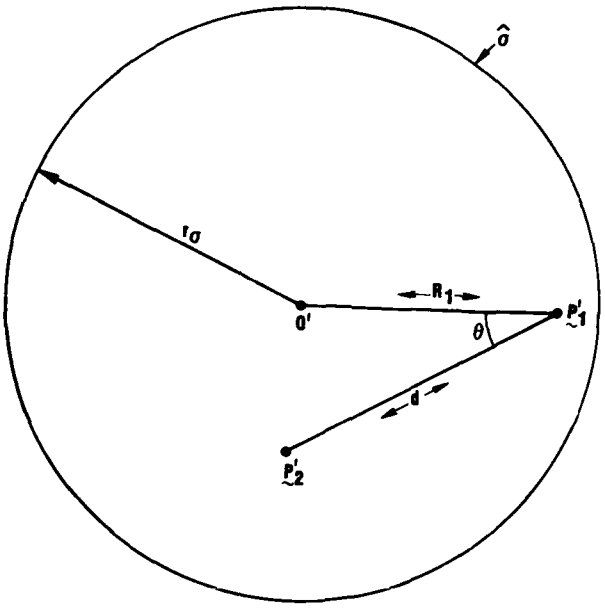

Figure 8. Geometry on observation plane for examining $J_B(\underset{\sim}{P}'_1, \underset{\sim}{P}'_2)$.

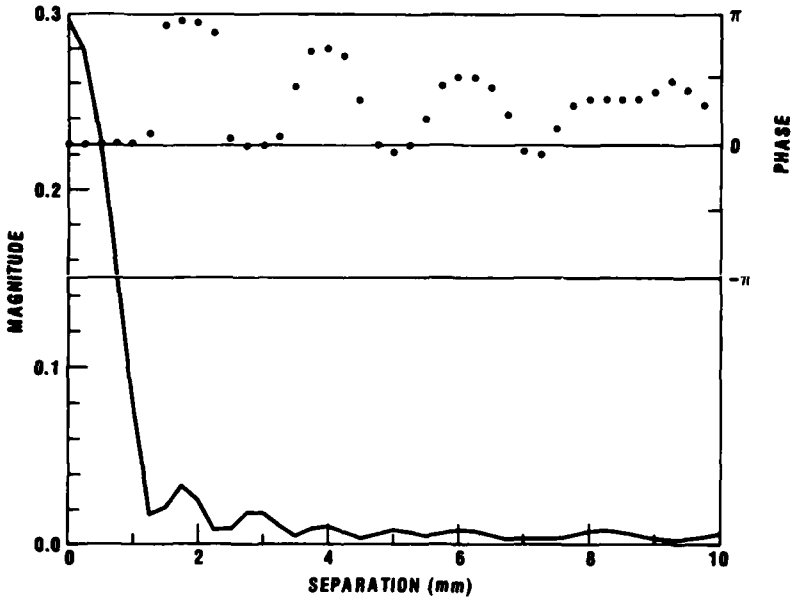

Figure 9. Mutual intensity versus observation point separation--fixed point at center.

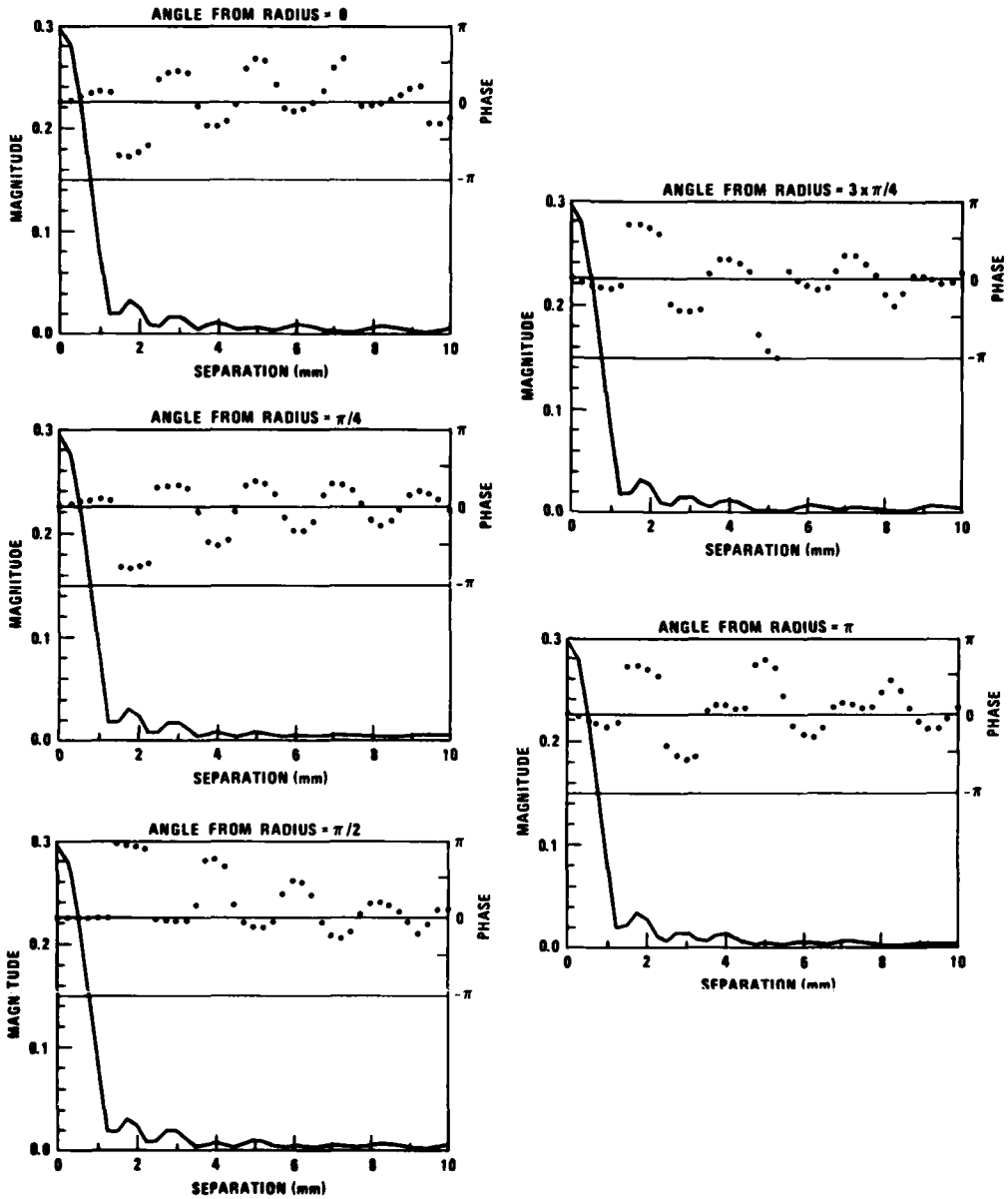

Figure 1[illegible]. Mutual intensity versus observation point separation--fixed point 1 cm from center.

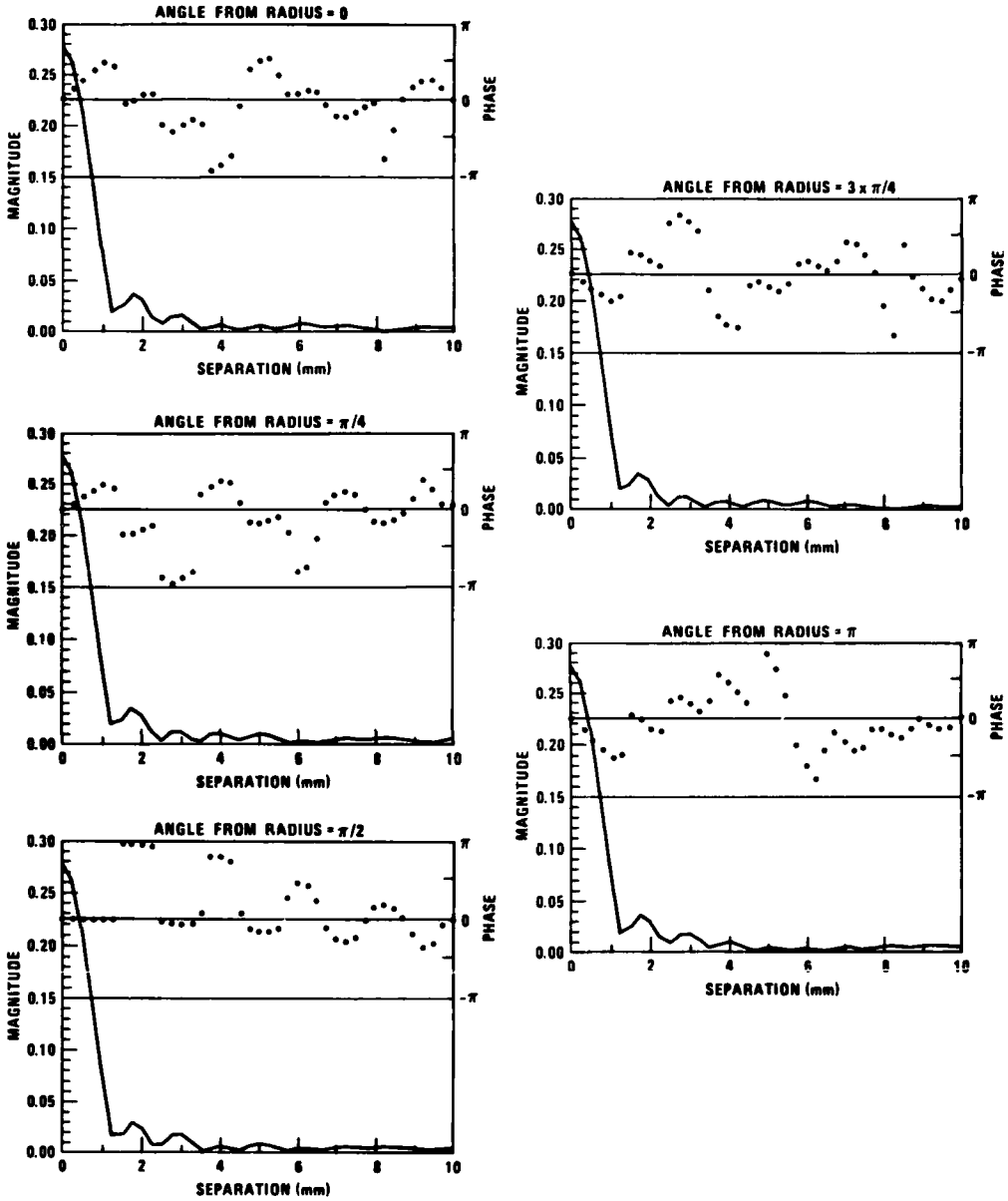

Figure 11. Mutual intensity versus observation point separation--fixed point 3 cm from center.

Figures 10 and 11 show the results when R_1 = 1 cm and R_1= 3 cm, respectively. For each of these cases, $\underset{\sim}{P}_2'$ was moved away from $\underset{\sim}{P}_1'$ at five angles, as indicated, from the radius passing through $\underset{\sim}{P}_1'$. As can be seen from the figures, the mutual intensity magnitude as a function of d (fig. 8) does not vary significantly for the various values of θ, nor for the three positions of $\underset{\sim}{P}_1'$. The mutual intensity phase, however, does show significant variation from case to case. In all cases, the phase exhibits very sharp jumps as d increases. However, the variation of the phase as a function of θ is noticeably more pronounced for R_1 = 3 cm (fig. 11) than for R_1 = 1 cm (fig. 10). Of course, the phase does not vary at all as a function of angle for R_1 = 0, since there is circular symmetry.

The characteristics of the mutual intensity can be described in general terms as follows. To a first approximation, the magnitude of the mutual intensity between two points within $\hat{\sigma}$ varies with d in the manner shown in figure 9, regardless of where the two points lie within $\hat{\sigma}$. The phase of the mutual intensity varies with d qualitatively, like the case when $\underset{\sim}{P}_1'$ is at the center of $\hat{\sigma}$. However, the phase is modulated by some perturbation function of θ for nonzero values of R_1. This perturbation becomes more strongly a function of θ as $\underset{\sim}{P}_1'$ is placed farther out. The specific nature of this perturbation is difficult to ascertain, however, from the calculations shown here.

The real part of J_B is of the most direct interest for optical heterodyne receiver analysis, which is the goal of the computational apparatus being discussed in this report. The major components of an optical heterodyne receiver are a photodetector/narrow-band amplifier combination and a local oscillator. The local oscillator is a highly coherent optical source that illuminates the photodetector at relatively high power levels, whose frequency is slightly shifted relative to that

of the received (target reflected) radiation. McGuire[7] has discussed the dependence of the average power output of such a receiver on the mutual intensity functions of the target-reflected radiation and the local oscillator field on the photodetector's active surface. He has found that the dependence is through only the real part of the product of the two mutual intensity functions. Since the mutual intensity function of the local oscillator is real and constant over the photodetector surface for normal-incidence, uniform-intensity plane-wave local oscillator beams, it follows that the heterodyne power depends on only the real part of J_B in such cases (assuming the photodetector lies in our observation plane).

Figures 12 to 14 show plots of the real part of $J_B(\underset{\sim}{P}_1', \underset{\sim}{P}_2')$ for the cases we have calculated. Despite the apparently discontinuous character of the phase of the mutual intensity as a function of d, the real part shows fairly regular behavior. In these figures, though, it is apparent that the dependence of phase on θ becomes much stronger as R_1 is increased. The dependence of phase on θ manifests itself as the spreading of the real part of the mutual intensity for the various values of θ plotted. Figure 14 shows the maximum spreading observed. It is interesting to notice that in figure 14 the behavior for $\theta = 0$ closely matches the behavior for $\theta = \pi$; similarly, the behavior for $\theta = \pi/4$ matches that for $\theta = 3\pi/4$. It thus might be a good first approximation to characterize the real part of the mutual intensity as follows. At $R_1 = 0$, the real part is a function of d as shown in figure 12 and has circular symmetry about $\underset{\sim}{P}_1'$. As R_1 increases, the real part remains similar in appearance, but the symmetry about $\underset{\sim}{P}_1'$ becomes elliptical, with the major axis of the ellipse of symmetry perpendicular to the radius through $\underset{\sim}{P}_1'$. The eccentricity of the ellipse increases with R_1.

---

[7] *Dennis W. McGuire, Coherent Detection of Partially Coherent Sources, Opt. Lett., 5, 2 (February 1980), 73-75.*

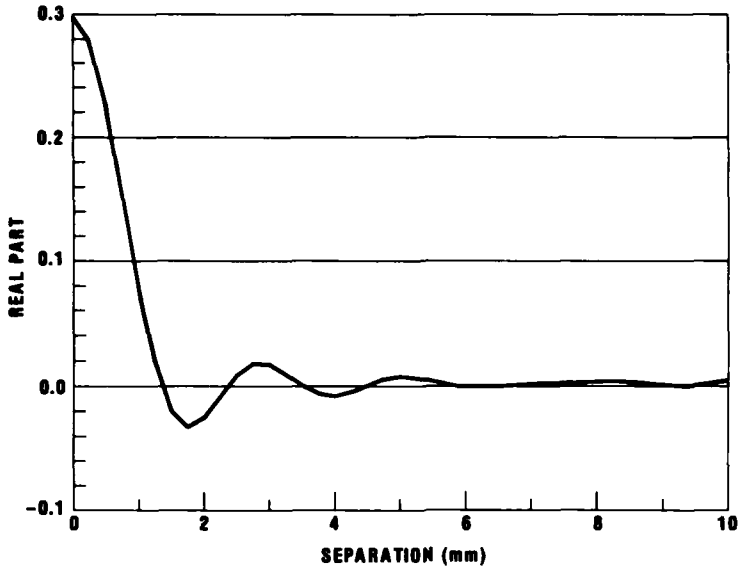

Figure 12. Mutual intensity versus observation point separation (real part)--fixed point at center.

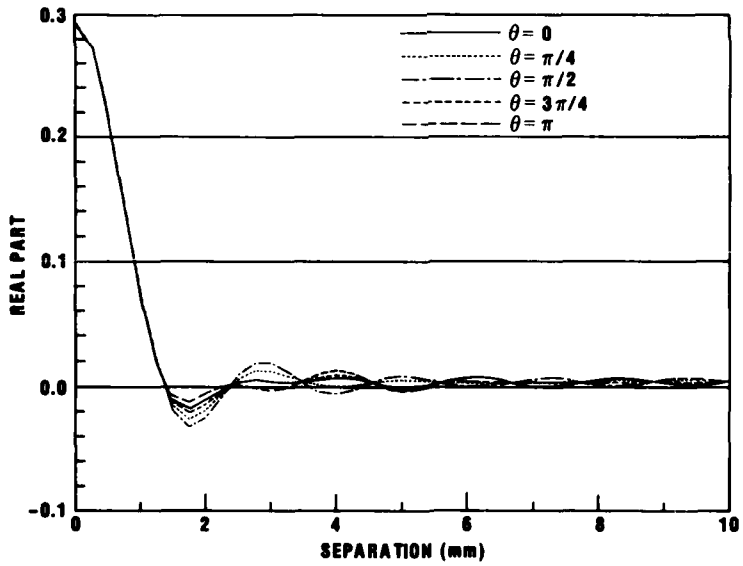

Figure 13. Mutual intensity versus observation point separation (real part)--fixed point 1 cm from center.

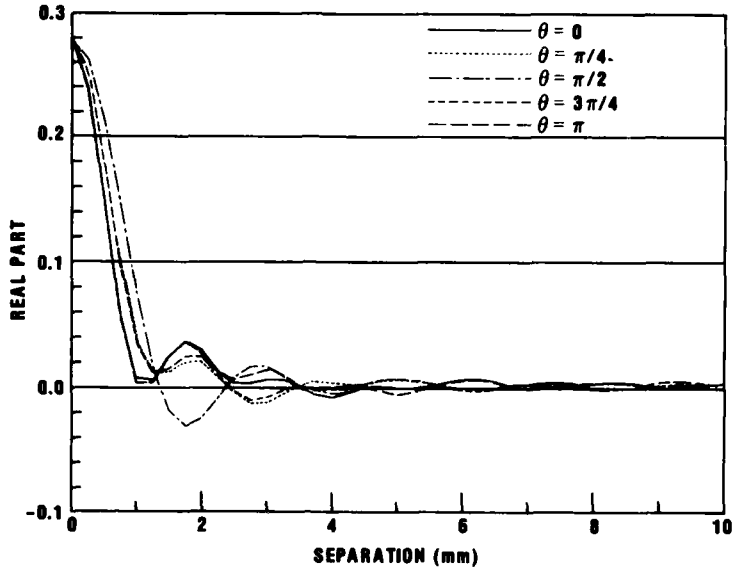

Figure 14. Mutual intensity versus observation point separation (real part)--fixed point 3 cm from center.

5. DISCUSSION

It is not the purpose of this report to quantitatively describe the mutual intensity function, but rather to describe how this function can be calculated. We have demonstrated that these calculations can be carried out within the limits set at the beginning of this report. However, as was stated earlier, these calculations are only a first step. The final objective is to examine the utility of optical heterodyne systems in laser fuzing systems. To this end, two areas of continued research are outlined.

The first area concerns a problem that should be considered in any future work, which is that a laser fuzing system generally contains a lens system in the receiver to collect and focus the received field onto a photodetector. The mutual intensity propagation equation considered in this report describes free-space propagation of light; it does not cope with propagation through lenses. Centered collecting optics can be

dealt with by calculating the mutual intensity at the entrance pupil, mapping the entrance pupil response to the exit pupil using principles of ray optics, and then propagating the mutual intensity at the exit pupil onto the observation plane (photodetector). The last step is quite problematic, however, because the mutual intensity at the exit pupil (the "target plane" for the second propagation calculation) is not necessarily dependent solely on $|\underset{\sim}{P}_1-\underset{\sim}{P}_2|$. At present, we have not investigated how this should be handled.

A related problem occurs in considering the power output from a photodetector in a heterodyne system. In this case, an expression involving the mutual intensity at the observation (detector) plane must be integrated over the detector surface. Again the function to be integrated would probably not be a function of $|\underset{\sim}{P}_1'-\underset{\sim}{P}_2'|$ alone. The integrand, however, is somewhat simpler, since no propagation, and hence no path length differences, are involved.

Both of the above calculations would be simplified considerably if the mutual intensity at the observation plane could be decomposed into a sum of appropriate radially dependent functions. Lens systems could then be dealt with using the techniques of this report. (However, edge effects, which we have not considered, may be too prominent in this case to be ignored.) Also, calculating detector power output would be reduced to calculating a sum of integrals, each of which is in essence a convolution of a radially dependent function with the detector surface. The first proposed area of future research is to investigate how, or if, mutual intensity functions calculated using the techniques of this report can be thus decomposed.

The second area of continued research is to develop a taxonomy and a catalog of responses to step-function mutual intensities. This would

allow a parametric characterization of the mutual intensity at an observation plane in terms of the cutoff radius r_c of $\hat{J}_\sigma(|\underset{\sim}{P}_1'-\underset{\sim}{P}_2'|, r_c)$ and geometrical parameters. Such a catalog would be the first step toward achieving a better understanding of the near-field behavior of the mutual intensity function, which is an essential feature for the heterodyne system analysis because of the relatively short detection ranges involved in fuzing. If this information were to be developed, many expensive intermediate calculations could be avoided.

ACKNOWLEDGEMENT

Arthur Hausner was invaluable to this investigation. His expertise in numerical analysis helped us find solutions to several numerical difficulties. In particular, it was he who suggested the change of variables in some of the integrals to avoid taking differences of large numbers. Without his help, many of the calculations would have been extremely difficult to perform.

LITERATURE CITED

(1) M. Born and E. Wolf, Principles of Optics, Ch 10, Pergamon Press (1970).

(2) M. Abramowitz and I. A. Stegun, Handbook of Mathematical Functions with Formulas, Graphs, and Mathematical Tables, NBS Applied Math Series 55 (1970).

(3) Theodore H. Hopp, A Routine for Numerical Evaluation of Integrals with Oscillation Behavior, Proceedings, 1979 Army Numerical Analysis and Computers Conference, El Paso, TX (1979).

(4) T. N. L. Patterson, The Optimum Addition of Points to Quadrature Formulae, Math. Comp., 22 (1968), 847-856.

(5) T. N. L. Patterson, Algorithm for Automatic Numerical Integration Over a Finite Interval, Algorithm 468 Comm. of the ACM, 16, 11 (November 1973), 694-699.

(6) J. W. Goodman, Statistical Properties of Laser Speckle Patterns, Laser Speckle and Related Phenomena, Ed., J. C. Dainty, Topics in Applied Physics, 9, Springer-Verlag (1975), 63-68.

(7) Dennis W. McGuire, Coherent Detection of Partially Coherent Sources, Op. Lett., 5, 2 (February 1980), 73-75.

APPENDIX A.--FORTRAN PROGRAM TO CALCULATE PROPAGATION OF MUTUAL INTENSITY FUNCTION

```
C       PROGRAM RAYS
C     PURPOSE
C       THIS PROGRAM CALCULATES THE MUTUAL INTENSITY BETWEEN TWO
C       POINTS, ONE BEING FIXED AND THE OTHER MOVING AWAY ALONG
C       SELECTED RAYS AT VARIOUS ANGLES FROM THE RADIUS.
C
C     USAGE
C       THIS PROGRAM REQUIRES A SET OF CONTROL CARDS ON LOGICAL UNIT
C       5 TO DIRECT THE CALCULATIONS.  THESE CARDS ARE AS FOLLOWS:
C          CARD #      CONTENTS      FORMAT
C            1          NPROB         I3
C           (2          RANGE         D15.7
C                       WAVE          D15.7
C                       RSIGMA        D15.7
C            3          RCORR         D15.7
C                       SIGMA2        D15.7
C            4          NPOSN         I3
C           (5          R1            D15.7
C                       ERR           D15.7
C                       ICD           I4
C            6          THSTEP        D15.7
C                       THSTRT        D15.7
C                       NTHSTP        I4
C            7          DSTEP         D15.7
C                       DSTART        D15.7
C                       NDSTEP        I4    ))
C       IN THE ABOVE, THE SEQUENCE OF CARDS AFTER CARD 1 IS REPEATED
C       NPROB TIMES (NPROB IS THE NUMBER OF PROBLEMS).  AFTER EACH
C       OCCURRENCE OF CARD 4 (ONCE IN EACH PROBLEM SET), CARDS 5
C       THROUGH 7 ARE REPEATED NPOSN TIMES (NPOSN IS THE NUMBER OF
C       SETS OF POSITIONS FOR OBSERVATION POINTS).
C
C       THE PROGRAM PERFORMS THE CALCULATION OF MUTUAL INTENSITY FOR
C       EACH PROBLEM AND EACH POINT PAIR AS INDICATED BY THE CONTROL
C       CARDS ABOVE.  THE POSITION OF THE OBSERVATION POINTS ARE
C       DETERMINED BY THE CONTENTS OF CARDS 5-7 AS FOLLOWS.  R1 IS THE
C       DISTANCE OF THE FIXED POINT FROM THE CENTER OF THE TARGET SIGMA.
C       (ERR AND ICD ARE EXPLAINED BELOW.)  THE SECOND POINT IS MOVED
C       AWAY FROM THE FIRST ALONG LINES AT VARIOUS ANGLES FROM THE RADIUS
C       PASSING THROUGH THE FIXED POINT.  THERE ARE NTHSTP OF THESE
C       LINES, AT ANGLES THSTRT, THSTRT+THSTEP, THSTRT+2*THSTEP, ETC.
C       ALONG EACH LINE, THE SECOND POINT IS LOCATED AT VARIOUS SEPA-
C       RATIONS FROM THE FIXED POINT.  THERE ARE NDSTEP POSITIONS FOR
C       THE SECOND POINT, AT SEPARATIONS OF DSTART, DSTART+DSTEP,
C       DSTART+2*DSTEP, ETC. FROM THE FIXED POINT.
C
C       THE VARIABLES ERR AND ICD ARE, RESPECTIVELY, THE REQUESTED
C       MAXIMUM RELATIVE ERROR OF THE NUMERICAL CALCULATIONS AND A
C       CODE REQUESTING THE CALCULATIONS DESIRED.  IF ICD=1, ONLY
C       THE RESIDUAL CONTRIBUTION TO THE MUTUAL INTENSITY IS CALCU-
C       LATED, OTHERWISE THE FULL MUTUAL INTENSITY BETWEEN EACH PAIR
C       OF OBSERVATION POINTS IS OBTAINED (WITHOUT, HOWEVER, THE EDGE
C       EFFECTS INCLUDED).
C
C       THE REMAINING VARIABLES ABOVE ARE AS FOLLOWS:
C          RANGE  - THE OBSERVATION DISTANCE FROM THE TARGET.
```

```
C         WAVE   - THE WAVELENGTH OF THE ILLUMINATING LIGHT.
C         RSIGMA - THE RADIUS OF THE TARGET.
C         RCORR  - THE PERFECT CORRELATION RADIUS.
C         SIGMA2 - THE VARIANCE OF THE SURFACE HEIGHT ROUGHNESS,
C                  SCALED TO THE WAVELENGTH.
C      ALL OF THESE QUANTITIES ARE INPUT IN METERS, EXCEPT SIGMA2,
C      WHICH IS DIMENSIONLESS.
C
C    NOTES
C      THIS PROGRAM WAS WRITTEN TO USE A VARIATION OF THE ROUTINE
C      IFEIX OF THE HDL PAGLOAD LIBRARY IN WHICH THE NAME FOFX
C      IS ASSUMED FOR THE SUBROUTINE WHICH COMPUTES THE INTEGRAND
C      FOR IFEIX.  THIS WAS DONE FOR THE SAKE OF RUNTIME EFFICIENCY.
C
C      IN ESTIMATING CPU TIME FOR THIS PROGRAM WHEN THE FULL MUTUAL
C      INTENSITY IS BEING CALCULATED, ALLOW 60 CPU SECONDS FOR EACH
C      POINT PAIR WHEN RUNNING ON THE 370/168 AFTER BEING COMPILED
C      WITH THE FORTRAN H-EXTENDED COMPILER WITH OPTIMIZATION LEVEL 2.
C
       IMPLICIT REAL*8 (A-H,O-Z)
       COMPLEX*16 JB,JRES
       REAL*8 JBMAG,JBPH
       COMMON /EVCM/RANGE,WAVEK,ERR/PROBLM/RSIGMA,RCORR,SIGMA2
       COMMON /PARM/D,R1,THETA
       DATA PI/3.14159265358979323846264 3D0/
       CALL PGMASK
C
C    READ NUMBER OF PROBLEMS AND LOOP FOR EACH PROBLEM.
C
       READ (5,5000) NPROB
5000   FORMAT (I3)
       DO 30 NP=1,NPROB
C
C    BEGIN PROCESSING - READ PROBLEM PARAMETERS
C
       READ (5,5010) RANGE,WAVE,RSIGMA,RCORR,SIGMA2
5010   FORMAT (3D15.7)
       WAVEK=2.D0*PI/WAVE
       WRITE (6,6000) RSIGMA,RANGE,RCORR,SIGMA2,WAVE
6000   FORMAT (' TARGET RADIUS=',2PF8.6,' CM, TARGET DISTANCE=',0PF5.0/
     *    ' CORRELATION RADIUS=',2PF10.8,' CM, SURFACE HEIGHT VARIANCE=',
     *    0PF9.4,', WAVELENGTH=',6PF6.2,' MICRONS')
C
C    READ NUMBER OF POSITION PARAMETER SETS; LOOP FOR EACH ONE.
C
       READ (5,5000) NPOSN
       DO 30 NPOS=1,NPOSN
       READ (5,5020) R1,ERR,ICD,THSTEP,THSTRT,NTHSTP,DSTEP,DSTART,NDSTEP
5020   FORMAT (2D15.7,I4)
       R1=DABS(R1)
C
C    COMPUTE ANGLE OF RAY FROM RADIUS - NORMALIZE TO BE BETWEEN (0,PI).
C
       DO 30 NTH=1,NTHSTP
       THETA=PI*(THSTRT+THSTEP*DFLOAT(NTH-1))
10     IF (THETA.GE.0.D0.AND.THETA.LE.PI) GO TO 20
       IF (THETA.LT.0.D0) THETA=THETA+PI
       IF (THETA.GT.PI) THETA=THETA-PI
       GO TO 10
C
```

```
C    STEP OUT ALONG EACH RAY - CALCULATE GEOMETRY
C
20     DO 30 ND=1,NDSTEP
       D=DSTART+DSTEP*DFLOAT(ND-1)
       X2=R1-D*DCOS(THETA)
       Y2=D*DSIN(THETA)
       R2=DSQRT(X2*X2+Y2*Y2)
       WRITE (6,6010) R1,X2,Y2,D
6010   FORMAT ('0OBSERVATION POINTS LOCATED AT (',2PF6.3,', 0.0  ), (',
     *   F6.3,',',F6.3,') CM.; SEPARATION =',F6.3,' CM.')
C
C    CALL GETANS TO OBTAIN RESIDUAL AND, IF DESIRED, TOTAL RESPONSE.
C    IF ICD=1, ONLY THE RESIDUAL IS COMPUTED, AND THE TOTAL IS SET
C    TO THIS VALUE; OTHERWISE, THE TOTAL RESPONSE INCLUDES THE SHORT
C    RANGE CORRELATION CONTRIBUTION.
C
       CALL GETANS(R1,R2,JRES,JB,ICD,ICHECK)
C
C    COMPUTE MAGNITUDE AND PHASE OF TOTAL RESPONSE AND PRINT ANSWER.
C
       JBMAG=CDABS(JB)
       JBPH=0.D0
       IF (JBMAG.GT.0.D0) JBPH=DATAN2(DIMAG(JB),DREAL(JB))/PI
       WRITE (6,6020) JRES,JB,JBMAG,JBPH
6020   FORMAT (' JRES=(',1PD15.8,',',D15.8,'), JB=(',D15.8,',',D15.8,
     *   '), MAG=',D15.8,', PHASE=',D15.8)
       IF (ICHECK.LT.0) WRITE (6,6030) ICHECK
6030   FORMAT (5X,'*** ICHECK =',I3,' ***')
30     CONTINUE
       STOP
       END
       SUBROUTINE GETANS(R1,R2,JRES,JB,ICD,ICHECK)
C    PURPOSE
C      THIS SUBROUTINE COMPUTES THE MUTUAL INTENSITY BETWEEN TWO
C      DATA POINTS, NEGLECTING EDGE EFFECTS.  IF ICD=1, ONLY THE RESIDUAL
C      CONTRIBUTION IS CALCULATED AND JB IS SET EQUAL TO JRES.
C
       IMPLICIT REAL*8 (A-H,O-Z)
       COMPLEX*16 EVJ,JB,JRES,QSUBAC,INTGND
       EXTERNAL INTGND
       COMMON /EVCM/RANGE,WAVEK,ERR/PROBLM/RSIGMA,RCORR,SIGMA2
       DATA PI/3.14159265358979323846264 3D0/
       RES=DEXP(-SIGMA2)
       RMAX=R1+RSIGMA-RCORR
       SCALE=(WAVEK*RANGE/(2.D0*PI))**2
C
C    CALCULATE SCALED RESIDUAL CORRELATION CONTRIBUTION
C
       JRES=RES*EVJ(R1,RSIGMA)*DCONJG(EVJ(R2,RSIGMA))
       JB=JRES
C
C    IF REQUESTED, INCLUDE THE CONTRIBUTION FROM SHORT RANGE
C    CORRELATION, EXCLUDING EDGE EFFECTS.
C
       IF (ICD.NE.1) JB=JRES+(1.D0-RES)*QSUBAC(0.D0,RMAX,ERR,NPTS,
     *   ICHECK,RELERR,INTGND)
       JB=SCALE*JB
       JRES=SCALE*JRES
       RETURN
       END
```

```
      COMPLEX FUNCTION INTGND*16(RADIUS)
C   PURPOSE
C     THIS FUNCTION EVALUATES THE INTEGRAND OF THE OUTERMOST INTEGRAL
C     FOR COMPUTING THE SHORT RANGE CORRELATION CONTRIBUTION TO THE
C     MUTUAL INTENSITY FUNCTION.
C
      IMPLICIT REAL*8 (A-H,O-Z)
      COMPLEX*16 EVJ,EVTH
      COMMON /PROBLM/RSIGMA,RCORR/EVCM/RANGE,WAVEK
      COMMON /PARM/D,R1,THETAR
      DATA PI/3.14159265358979323846264 3D0/
C
C   EVALUATE FIRST FACTOR OF INTEGRAND - RESIDUAL FROM A
C   SMALL CIRCLE.
C
      INTGND=RADIUS*EVJ(RADIUS,RCORR)
C
C   EVALUATE SECOND FACTOR OF INTEGRAND - AN INTEGRAL IN THETA
C
      IF (RADIUS.GT.RSIGMA-RCORR-R1) GO TO 10
C
C   TEST FOR DEGENERATE CASE
C
      THETA1=PI
      IF (D.EQ.0.D0) GO TO 50
C
C   INTEGRAL IN THETA IS OVER A FULL CIRCLE - INTEGRAND IS TWICE
C   THE INTEGRAL FROM 0 TO PI IN THETA, TIMES THE FIRST FACTOR.
C
      INTGND=INTGND*2.D0*EVTH(RADIUS,1.D0,-1.D0)
      RETURN
C
C   INTEGRAL IN THETA IS OVER LESS THAN A FULL CIRCLE - SELECT
C   THE RIGHT BREAKUP OF THIS INTEGRAL AND COMPUTE INTEGRAND
C   AS THE PRODUCT OF THIS INTEGRAL WITH THE FIRST FACTOR.
C   FIRST, FIND THE ENDPOINTS OF THE INTEGRATION IN THETA.  THE
C   ENDPOINTS ARE THETAR-THETA1 AND THETAR+THETA1.
C
10    X1=(RADIUS*RADIUS+R1*R1-(RSIGMA-RCORR)**2)/(2.D0*R1*RADIUS)
      THETA1=DARCOS(X1)
      IF (D.EQ.0.D0) GO TO 50
      XR=DCOS(THETAR)
      XA=X1*XR-DSQRT((1.D0-X1*X1)*(1.D0-XR*XR))
      XB=X1*XR+DSQRT((1.D0-X1*X1)*(1.D0-XR*XR))
      IF (THETAR-THETA1.LT.0.D0.AND.THETAR+THETA1.LE.PI) GO TO 20
      IF (THETAR-THETA1.GE.0.D0.AND.THETAR+THETA1.GT.PI) GO TO 30
      IF (THETAR-THETA1.LT.0.D0.AND.THETAR+THETA1.GT.PI) GO TO 40
C
C   CASE 1 - 0 <= THETAR-THETA1 <= THETAR+THETA1 <= PI
C
      INTGND=INTGND*EVTH(RADIUS,XB,XA)
      RETURN
C
C   CASE 2 - THETAR-THETA1 < 0 <= THETAR+THETA1 <= PI
C
20    INTGND=INTGND*(2.D0*EVTH(RADIUS,1.D0,XB)+EVTH(RADIUS,XB,XA))
      RETURN
C
C   CASE 3 - 0 <= THETAR-THETA1 <= PI < THETAR+THETA1
C
```

```
30    INTGND=INTGND*(EVTH(RADIUS,XB,XA)+2.D0*EVTH(RADIUS,XA,-1.D0))
      RETURN
C
C   CASE 4 - THETAR-THETA1 < 0 < PI < THETAR+THETA1
C
40    INTGND=INTGND*(2.D0*EVTH(RADIUS,1.D0,XB)+
     *   EVTH(RADIUS,XB,XA)+2.D0*EVTH(RADIUS,XA,-1.D0))
      RETURN
C
C   DEGENERATE CASE - INTEGRAL IN THETA CAN BE COMPUTED DIRECTLY
C
50    INTGND=INTGND*2.D0*THETA1*CDEXP(DCMPLX(0.D0,-WAVEK*
     *   DSQRT(RANGE**2+RADIUS**2)))/(RANGE**2+RADIUS**2)
      RETURN
      END
      COMPLEX FUNCTION EVJ*16(R,RADIUS)
C   PURPOSE
C     THIS SUBROUTINE CALCULATES THE MUTUAL INTENSITY FUNCTION FOR
C     POINTS SEPARATED BY A DISTANCE 'R' FROM A TARGET OF RADIUS
C     'RADIUS'.
C
      IMPLICIT REAL*8 (A-H,O-Z)
      COMPLEX*16 D,Z
      COMMON /EVCM/RANGE,WAVEK,ERR/EVJCM/RAD,OFFSET
      COMMON /CONTRL/ISWTCH
      LOGICAL LONG
      DATA PI/3.14159265358979323846264 3D0/
C
      F(X)=(1.D0-2.D0*(1.D0-1.2D1*(1.D0-3.D1/(X*X))/(X*X))/(X*X))/X
      G(X)=(1.D0-6.D0*(1.D0-2.D1*(1.D0-4.2D1/(X*X))/(X*X))/(X*X))/(X*X)
C
      RAD=RADIUS
      OFFSET=R
      Z=CDEXP(DCMPLX(0.D0,WAVEK*RANGE))
      LONG=(RADIUS-R).LT.1.D-2*RANGE
      SKD=((RADIUS-R)/RANGE)**2
      A=WAVEK*RANGE*(DSQRT(1.D0+SKD)-1.D0)
      IF (LONG) A=WAVEK*RANGE*SKD*(1.D0-SKD*(1.D0-SKD/2.D0)/4.D0)/2.D0
      SKD=WAVEK*RANGE*DSQRT(1.D0+SKD)
C
C   CALCULATE CONTRIBUTION FROM INSIDE TARGET CYLINDER (IF ANY).
C
      D=(0.D0,0.D0)
      IF (R.LT.RADIUS) D=2.D0*PI*Z*DCMPLX(
     *   G(WAVEK*RANGE)+F(SKD)*DSIN(A)-G(SKD)*DCOS(A),
     *   F(WAVEK*RANGE)-F(SKD)*DCOS(A)-G(SKD)*DSIN(A))
C
C   CALCULATE REMAINDER OF CONTRIBUTIONS
C
      B=((RADIUS+R)/RANGE)**2
      IF (LONG) B=WAVEK*RANGE*B*(1.D0-B*(1.D0-B/2.D0)/4.D0)/2.D0
      IF (.NOT.LONG) B=WAVEK*RANGE*(DSQRT(1.D0+B)-1.D0)
      ISWTCH=1
      IER=1
      CALL IFEIX(EREAL,EIMAG,A,B,100000,.1D0*ERR,0,0,IER)
      IF (IER.EQ.2) GO TO 10
      EVJ=D+2.D0*Z*DCMPLX(EREAL,EIMAG)
      RETURN
10    WRITE (6,6010) R,RADIUS,A
6010  FORMAT (' IFEIX DID NOT CONVERGE - CALLED FROM EVJ.'/
```

```
     *    ' VARIABLES ARE: R=',1PD13.6,', RADIUS=',D13.6,
     *    ', A=',D13.6/' PROGRAM STOPPED')
      STOP
      END
      COMPLEX FUNCTION EVTH*16(OFFSET,COS0,COS1)
C   PURPOSE
C     THIS SUBROUTINE COMPUTES THE MUTUAL INTENSITY DUE TO SHORT
C     RANGE CORRELATION FROM A TARGET, WITH ONE OBSERVATION POINT
C     SEPARATED BY 'D' FROM THE OTHER ONE.
C
      IMPLICIT REAL*8 (A-H,O-Z)
      LOGICAL LONG
      COMMON /EVCM/RANGE,WAVEK,ERR/EVTHCM/A,B,BLESSA
      COMMON /CONTRL/ISWTCH/PARM/D
      LONG=((D-OFFSET)/RANGE)**2.LT.1.D-3
      A=WAVEK*DSQRT(RANGE**2+(D-OFFSET)**2)
      B=WAVEK*DSQRT(RANGE**2+(D+OFFSET)**2)
      BLESSA=B-A
      IF (LONG) BLESSA=
     *   2.D0*WAVEK*D*OFFSET*(1.D0-(OFFSET**2+D**2)*
     *   (1.D0-(OFFSET**2+D**2)/RANGE**2)/(2.D0*RANGE**2)-
     *   (OFFSET**2-D**2)**2/(8.D0*RANGE**4))/RANGE
C
C   TEST IF NEAR TOP OF INTERVAL (A,B)
C
      IF (COS0.LT.0.D0) GO TO 30
C
C   NEAR BOTTOM END - TEST IF LONG RANGE APPROXIMATION SHOULD BE USED.
C
      IF (LONG) GO TO 10
C
C   USE SHORT RANGE EQUATIONS.
C
      X0=WAVEK*DSQRT(RANGE**2+D**2+OFFSET**2-2.D0*D*OFFSET*COS0)-A
      X1=WAVEK*DSQRT(RANGE**2+D**2+OFFSET**2-2.D0*D*OFFSET*COS1)-A
      GO TO 20
C
C   USE LONG RANGE EQUATIONS WITH INTERVAL NOT NEAR TOP END OF (A,B)
C
10    X0=D*OFFSET*(1.D0-COS0)
      X1=D*OFFSET*(1.D0-COS1)
      X=(D-OFFSET)**2
      X0=WAVEK*X0*(1.D0-(X+X0)*(1.D0-(X+X0)/RANGE**2)/(2.D0*RANGE**2)-
     *   X*(X+2.D0*X0)/(8.D0*RANGE**4))/RANGE
      X1=WAVEK*X1*(1.D0-(X+X1)*(1.D0-(X+X1)/RANGE**2)/(2.D0*RANGE**2)-
     *   X*(X+2.D0*X1)/(8.D0*RANGE**4))/RANGE
20    X0=DMIN1(BLESSA,DMAX1(X0,0.D0))
      X1=DMAX1(0.D0,DMIN1(X1,BLESSA))
      ISWTCH=2
      IER=1
      CALL IFBIX(ANSR,ANSI,X0,X1,100000,.1D0*ERR,0,0,IER)
      IF (IER.EQ.2) GO TO 60
      EVTH=2.D0*WAVEK**2*DCMPLX(ANSR,-ANSI)*CDEXP(DCMPLX(0.D0,-A))
      RETURN
C
C   NEAR TOP END - TEST IF LONG RANGE APPROXIMATION SHOULD BE USED.
C
30    IF (LONG) GO TO 40
      X0=WAVEK*DSQRT(RANGE**2+D**2+OFFSET**2-2.D0*D*OFFSET*COS0)-B
      X1=WAVEK*DSQRT(RANGE**2+D**2+OFFSET**2-2.D0*D*OFFSET*COS1)-B
```

```
      GO TO 50
C
C   USE LONG RANGE EQUATIONS WITH INTERVAL NEAR TOP END OF (A,B)
C
40    X0=-D*OFFSET*(1.D0+COS0)
      X1=-D*OFFSET*(1.D0+COS1)
      X=(D+OFFSET)**2
      X0=WAVEK*X0*(1.D0-(X+X0)*(1.D0-(X+X0)/RANGE**2)/(2.D0*RANGE**2)-
     *   X*(X+2.D0*X0)/(8.D0*RANGE**4))/RANGE
      X1=WAVEK*X1*(1.D0-(X+X1)*(1.D0-(X+X1)/RANGE**2)/(2.D0*RANGE**2)-
     *   X*(X+2.D0*X1)/(8.D0*RANGE**4))/RANGE
50    X0=DMAX1(-BLESSA,DMIN1(X0,0.D0))
      X1=DMIN1(0.D0,DMAX1(X1,-BLESSA))
      ISWTCH=3
      IER=1
      CALL IFBIX(ANSR,ANSI,X0,X1,100000,.1D0*ERR,0,0,IER)
      IF (IER.EQ.2) GO TO 60
      EVTH=2.D0*WAVEK**2*DCMPLX(ANSR,-ANSI)*CDEXP(DCMPLX(0.D0,-B))
      RETURN
60    PRINT *,OFFSET,COS0,COS1,A,B,BLESSA,ISWTCH,X0,X1
      STOP
      END
      SUBROUTINE FOPX(X,Y)
      IMPLICIT REAL*8 (A-H,O-Z)
      COMMON /EVCM/RANGE,WAVEK/EVJCM/R,S
      COMMON /EVTRCM/A,B,BLESSA/CONTRL/ISWTCH
      COMMON /CMSPLT/A0
      IOPT=0
      GO TO (10,20,30),ISWTCH
      STOP 1
C
C   INTEGRAND FOR EVJ
C
10    Y=X/WAVEK
      Y=(Y*Y+2.D0*RANGE*Y+S*S-R*R)/(2.D0*S*DSQRT(Y*Y+2.D0*RANGE*Y))
      IF (DABS(Y).GT.1.D0) Y=DSIGN(1.D0,Y)
      Y=DARCOS(Y)/(X+WAVEK*RANGE)
      GO TO 40
C
C   INTEGRAND FOR EVTH
C
20    Y=1.D0/((X+A)*DSQRT(X*(BLESSA-X)*(X+A+B)*(X+2.D0*A)))
      GO TO 40
C
C   INTEGRAND FOR EVTH - TOP OF (A,B)
C
30    Y=1.D0/((X+B)*DSQRT(-X*(X+BLESSA)*(X+A+B)*(X+2.D0*B)))
40    IF (IOPT.EQ.1) Y=Y*(1.D0+DCOS(X-A0))
      IF (IOPT.EQ.2) Y=Y*(1.D0+DSIN(X-A0))
      IF (IOPT.EQ.3) Y=Y*DCOS(X)
      IF (IOPT.EQ.4) Y=Y*DSIN(X)
      RETURN
      ENTRY FCOSXA(X,Y)
      IOPT=1
      GO TO (10,20,30),ISWTCH
      STOP 1
      ENTRY FSINXA(X,Y)
      IOPT=2
      GO TO (10,20,30),ISWTCH
      STOP 1
```

APPENDIX A

```
      ENTRY FCOSX(X,Y)
      IOPT=3
      GO TO (10,20,30),ISWTCH
      STOP 1
      ENTRY FSINX(X,Y)
      IOPT=4
      GO TO (10,20,30),ISWTCH
      STOP 1
      END
```

DISTRIBUTION

ADMINISTRATOR
DEFENSE TECHNICAL INFORMATION CENTER
ATTN DTIC-DDA (12 COPIES)
CAMERON STATION, BUILDING 5
ALEXANDRIA, VA 22314

COMMANDER
US ARMY RSCH & STD GP (EUR)
ATTN CHIEF, PHYSICS & MATH BRANCH
FPO NEW YORK 09510

COMMANDER
US ARMY MISSILE & MUNITIONS
CENTER & SCHOOL
ATTN ATSK-CTD-F
REDSTONE ARSENAL, AL 35809

DIRECTOR
US ARMY MATERIEL SYSTEMS ANALYSIS ACTIVITY
ATTN DRXSY-MP
ABERDEEN PROVING GROUND, MD 21005

DIRECTOR
US ARMY BALLISTIC RESEARCH LABORATORY
ATTN DRDAR-TSB-S (STINFO)
ABERDEEN PROVING GROUND, MD 21005

TELEDYNE BROWN ENGINEERING
CUMMINGS RESEARCH PARK
ATTN DR. MELVIN L. PRICE, MS-44
HUNTSVILLE, AL 35807

ENGINEERING SOCIETIES LIBRARY
ATTN ACQUISITIONS DEPARTMENT
345 E. 47TH STREET
NEW YORK, NY 10017

HQ, USAF/SAMI
WASHINGTON, DC 20330

US ARMY ELECTRONICS TECHNOLOGY
& DEVICES LABORATORY
ATTN DELET-DD
FT MONMOUTH, NJ 07703

COMMANDER
US ARMY ARMAMENT RESEARCH
& DEVELOPMENT COMMAND
ATTN DRDAR-SE, SYSTEMS EVALUATION
OFFICE, LTC GRADY COOK
ATTN DRDAR-LCN-C, G. TAYLOR
ATTN DRDAR-AS, R. ANDREJZOVICS
DOVER, NJ 07801

DIRECTOR
NIGHT VISION & ELECTRO-OPTICS
LABORATORY
ATTN DELNV-V (2 COPIES)
ATTN DELNV-R, R. BUSER
FT BELVOIR, VA 22060

COMMANDER/DIRECTOR
ATMOSPHERIC SCIENCES LABORATORY
ATTN DELAS-EO, F. NILES
WHITE SANDS MISSILE RANGE, NM 88002

COMMANDER
US ARMY MISSLE COMMAND
ATTN DRSMI-REM, H. ANDERSON
REDSTONE ARSENAL, AL 35898

ENVIRONMENTAL RESEARCH INSTITUTE
OF MICHIGAN
PO BOX 8618
ATTN IRIA LIBRARY
ANN ARBOR, MI 48107

COMMANDER
NAVAL WEAPONS CENTER
ATTN CODE 3311, K. BULLOCK (4 COPIES)
ATTN CODE 3311, J. CRISLER
CHINA LAKE, CA 93555

COMMANDER
AFATL
ATTN L. STABLES
EGLIN AIR FORCE BASE, FL 32542

COMMANDER
AFAL/TEO
ATTN R. HARRIS
WRIGHT-PATTERSON AF BASE, OH 45433

MOTOROLA, INC
GOVERNMENT ELECTRONICS DIVISON
ATTN A. GARAS (2 COPIES)
PO BOX 1417
8201 E. MCDOWEL RD
SCOTTSDALE, AZ 85252

SANTA BARBARA RESEARCH CENTER
ATTN N. RIGBY (2 COPIES)
75 COROMAR DRIVE
GOLETA, CA 93117

NATIONAL BUREAU OF STANDARDS
ATTN THEODORE H. HOPP (10 COPIES)
ROUTE 270 & QUINCE ORCHARD RD
GAITHERSBURG, MD 20760

DISTRIBUTION (Cont'd)

US ARMY ELECTRONICS RESEARCH
& DEVELOPMENT COMMAND
ATTN TECHNICAL DIRECTOR, DRDEL-CT

HARRY DIAMOND LABORATORIES
ATTN CO/TD/TSO/DIVISION DIRECTORS
ATTN RECORD COPY, 81200
ATTN HDL LIBRARY, 81100 (2 COPIES)
ATTN HDL LIBRARY, 81100 (WOODBRIDGE)
ATTN TECHNICAL REPORTS BRANCH, 81300
ATTN CHAIRMAN, EDITORIAL COMMITTEE
ATTN LEGAL OFFICE, 97000
ATTN MORRISON, R., 13500 (GIDEP)
ATTN CHIEF, 13000
ATTN CHIEF, 11000
ATTN CHIEF, 13300
ATTN CHIEF, 11400
ATTN COX, L., 00211
ATTN HUMPHREY, R., 13300
ATTN GRIFFIN, J. R., 21100
ATTN HATTERY, W. V., 13300
ATTN SANN, K. H., 15000
ATTN PEPERONE, S., 36000
ATTN DOBRIANSKY, B., 13500 (2 COPIES)
ATTN LANHAM, C., 00213
ATTN GIGLIO, D., 15300
ATTN GEIPE, T., 22100
ATTN TUTTLE, J., 21400
ATTN VANDERWALL, J., 22800
ATTN CONNER, M., 15200
ATTN TOZZI, L., 34000
ATTN SOLN, J. R., 22300
ATTN BRANDT, H., 22300
ATTN MCGUIRE, D., 13300 (10 COPIES)

END

FILMED

2-83

DTIC